Journal of Rock Mechanics and Geotechnical Engineering 18 (2026) 3407–3424

Contents lists available at ScienceDirect

Journal of Rock Mechanics and Geotechnical Engineering

journal homepage: www.jrmge.cn

Full Length Article

Consolidation and mechanical response of cemented tailings backfill to multiaxial stresses from rockwall closure and self-loading

Hongbin Liu, Mamadou Fall *

Department of Civil Engineering, University of Ottawa, Ottawa, ON, K1N 6N5, Canada

ARTICLE INFO

Article history:
Received 11 February 2025
Received in revised form
2 July 2025
Accepted 9 July 2025
Available online 13 October 2025

Keywords:
Consolidation behaviour
Cemented paste backfill (CPB)
Tailings
Multiaxial stresses curing
Mine
Rockwall closure

ABSTRACT

Cemented paste backfill (CPB) is a key material in underground mining, providing essential ground support while aiding in tailings management. However, current research has overlooked the combined effects of horizontal rockwall closure stress and vertical self-loading stress, referred to as multiaxial stress, on the CPB's consolidation behavior and its mechanical properties development. Understanding and assessing these effects is critical because they directly affect the stability and performance of CPB structures. In this study, a novel multiaxial compressive stress curing and monitoring apparatus was used to simulate two horizontal rockwall closure scenarios with a consistent backfilling rate, under both drained and undrained conditions. Key parameters assessed included unconfined compressive strength (UCS), deformation during curing, stress-strain behavior, and modulus of elasticity. The results highlight that rockwall closure, combined with vertical stress, plays a pivotal role in the consolidation behavior of CPB, significantly affecting key mechanical properties. Higher horizontal stress from faster rockwall closure intensified compression during curing, leading to reduced porosity, enhanced particle rearrangement, and accelerated consolidation. This intensified consolidation leads to notable improvements in mechanical properties, including increased UCS, enhanced stiffness, and a higher modulus of elasticity, indicating improved load-bearing capacity. Moreover, the interaction between multiaxial stress and drainage conditions influenced stress-strain behavior and deformation, with drained conditions promoting earlier plasticity and higher peak stresses. These findings underscore the critical influence of multiaxial stress, combined with drainage conditions, on CPB performance, offering valuable insights for optimizing CPB design in underground mining applications.

1. Introduction

In underground mining, the backfilling process involves filling the voids or stopes created by ore extraction with a material known as backfill (Gric, 2001; Kesimal et al., 2005; Fall et al., 2008; Wu et al., 2018; Yang et al., 2023). This process is essential for maintaining mine stability, preventing ground subsidence, and minimizing the environmental impact of mining operations. Without backfilling, the underground voids left behind can lead to progressive surface subsidence, ground cracking, and collapse, causing severe damage to surface infrastructure and posing significant risks to human safety (Sun et al., 2018). Even when backfilling is employed, failure of the backfill material—particularly during early exposure or due to insufficient strength development—can compromise stope stability, trigger secondary collapses, and undermine the overall structural integrity of the mine (Cui and Fall, 2018; Zhao et al., 2020). These risks highlight the critical need for reliable and durable backfill systems in underground mining operations. Cemented paste backfill (CPB) has emerged as a promising and cost-effective solution for supporting stopes and managing tailings in mines (Fang and Fall, 2019; Yin et al., 2020; Wu et al., 2022; Wang et al., 2022a; Ruan et al., 2023; Lu et al., 2024b). CPB typically consists of mine tailings, cement, water, and sometimes additives to enhance its performance. These components are thoroughly mixed at a backfill plant to create a homogeneous paste. Once prepared, the backfill material is transported, typically via pipelines, to the underground stopes, where it is placed to stabilize the mine structure (Cheng

* Corresponding author.
E-mail address: mfall@uottawa.ca (M. Fall).

Peer review under responsibility of Institute of Rock and Soil Mechanics, Chinese Academy of Sciences.

https://doi.org/10.1016/j.jrmge.2025.07.013

et al., 2020; Ruan et al., 2021; Yin et al., 2021; Song et al., 2022; Wang et al., 2022a, 2024; Yang et al., 2024).

In underground stopes, CPB is subjected to various curing conditions that significantly influence its performance and strength development. These conditions include thermal, hydraulic, mechanical, and chemical factors, collectively referred to as thermal-hydraulic-mechanical-chemical (THMC) conditions (Cui and Fall, 2017b). Temperature fluctuations within the mine can directly impact the rate of cement hydration, influencing the speed of the strength development (Rawlings and Phillips, 2001; Fall and Samb, 2009; Fall et al., 2014; Wu et al., 2014, 2025; Maurya et al., 2015; Fang and Fall, 2018, 2020; Xu et al., 2020; Zhou and Fall, 2023; Xue et al., 2023). The presence of water, whether from groundwater inflow or residual water in the CPB, plays a crucial role in the curing process, affecting consolidation and stability (Sivakugan, 2008; Hasan et al., 2013; Sun et al., 2017, 2019; Jaouhar and Li, 2019; Wang et al., 2022b; Song et al., 2023; Ma et al., 2023; Lu et al., 2024a). Vertical stress from the self-weight of the overlying CPB material and overburden from the overlying rock (Yan et al., 2025), along with horizontal stress from the convergence of the surrounding rock mass – known as rockwall closure (see Fig. 1) – further influence the compaction, deformation, and strength of the backfill (Raffaldi et al., 2019; Liu and Fall, 2024). Additionally, the chemical environment within the mine, including the presence of sulfates, chlorides, or other reactive substances in the tailings or mine water, can significantly interact with the cement in CPB, potentially forming detrimental compounds that affect the durability and long-term strength of the material (Benzaazoua et al., 2002; Li and Fall, 2016; Aldhafeeri and Fall, 2017; Naidu et al., 2019; Sari et al., 2022; Wang et al., 2024; He et al., 2025). Among THMC conditions, mechanical conditions in deep underground mines become more challenging to the backfill as the mining depth increases. In real-world scenarios, CPB can be subjected to vertical stresses exceeding 4 MPa due to stope heights reaching up to 200 m, and additional vertical stresses from mining activities can raise in-situ stresses to several tens of megapascals. Moreover, significant rockwall closures are frequently encountered, exerting horizontal stresses exceeding 5 MPa in mines over 2000 m deep (Seymour et al., 2017; Raffaldi et al., 2019; Liu and Fall, 2024). The effect of these high in situ stresses on the curing behavior of CPB is still not well understood, highlighting the need for further research in this area.

Consolidation, a key aspect of CPB's performance, generally refers to the volume change resulting from the expulsion of water from its pores under applied stress. Under drained conditions, the vertical and horizontal stresses from the overlying material and surrounding rock cause the pore water within the CPB to be squeezed out, leading to a denser and more compact structure over time. Under undrained conditions, although the pore water cannot be expelled, the cement in CPB consumes water through hydration reactions – a process known as self-desiccation (Grabinsky et al., 2006; Wang et al., 2016; Tian and Fall, 2021). This reduction in pore water content causes the CPB to experience consolidation even under undrained conditions. Therefore, CPB undergoes consolidation under both drained and undrained conditions, albeit through different mechanisms.

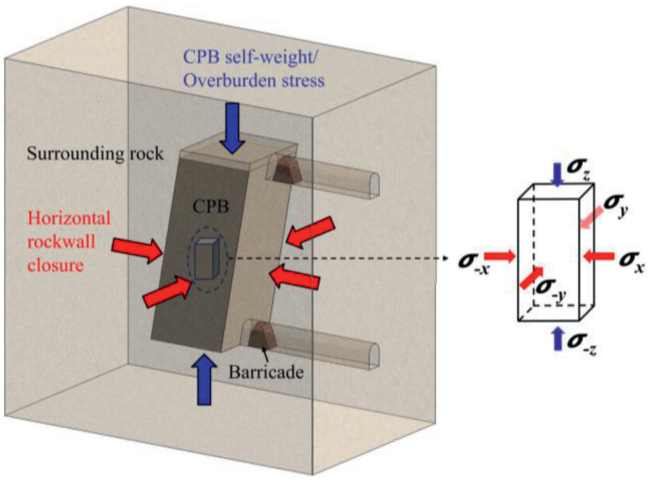

Fig. 1. Schematic representation of CPB interaction with surrounding rock.

The consolidation process is crucial for the development of strength and stability in CPB, as it directly influences the rate at which the material gains strength and its ability to support the surrounding rock mass in underground mining operations. The one-dimensional (1D) consolidation behavior of CPB has been extensively studied, focusing on various factors such as binder content, curing time, drainage conditions, and the influence of multiphysics processes (Yilmaz et al., 2008, 2015; Belem et al., 2016; Cui and Fall, 2017a; Wang et al., 2018; Jaouhar and Li, 2019; Jafari et al., 2020). These studies have provided valuable insights into how CPB consolidates in underground mining conditions and how this affects its mechanical performance and design. For instance, research has shown that an increase in binder content generally leads to a higher coefficient of consolidation (C_v) and a decrease in compressibility parameters, improving the mechanical strength of CPB over time (Yilmaz et al., 2008). Drainage conditions also play a significant role, with well-drained conditions enhancing consolidation by reducing pore water pressure and increasing settlement (Belem et al., 2016; Cui and Fall, 2018). To better guide CPB design, researchers have also attempted to model the consolidation behavior of CPB. For example, Fahey et al. (2010) applied Gibson's solution, a classical consolidation theory, to understand the consolidation behavior during the backfilling process. They highlighted the limitations of this solution, particularly its assumption of constant C_v and the 1D nature of the model, which does not fully capture the complexities of CPB consolidation in three-dimensional (3D) stope geometries. Similarly, Cui and Fall (2017a) expanded the understanding of CPB consolidation by incorporating THMC processes into their models. They demonstrated that traditional consolidation models, which primarily focus on hydraulic and mechanical coupling, are inadequate for predicting CPB behavior. Their 3D coupled multiphysics model, validated against experimental data, provided a more comprehensive understanding of the complex interactions during CPB consolidation.

However, most of the existing models have relied on 1D consolidation tests to derive their conclusions. While these models have advanced our understanding of CPB behavior, they are inherently limited by their 1D approach, which does not fully capture the complexities of real-world conditions in underground stopes, particularly in deep mines, where stresses are often multidirectional and vary over time. Consequently, the consolidation behavior of CPB under high vertical and horizontal rockwall closure stress conditions remains poorly understood. Key questions, such as how CPB consolidates under time-dependent multiaxial stresses and how drainage conditions affect this process, have not been addressed. These questions are critical for understanding and predicting the performance of CPB in deep mining environments, where multiaxial high-stress conditions can pose significant safety concerns.

While the effects of vertical self-weight and horizontal rockwall closure stresses on CPB properties (particularly strength) have been individually explored in the literature (e.g. Yilmaz et al., 2014;

Ghirian and Fall, 2016; Belem et al., 2016; Zhao et al., 2021; Chen et al., 2022; Al-Moselly and Fall, 2022, 2024a), the combined influence of these multiaxial stress conditions on CPB performance – especially in conjunction with varying drainage scenarios – remains significantly underexplored. Almost all prior studies have relied on 1D consolidation frameworks (e.g. Yilmaz et al., 2008, 2015; Shahsavari and Grabinsky, 2014; Wang et al., 2018; Jafari et al., 2020), overlooking the complex, multidirectional (3D) stress interactions and their interplay with drainage behavior that CPB materials experience in deep mine environments. Moreover, existing studies and models often neglect the role of horizontal closure-induced stress development over time, as well as how drainage availability modulates consolidation mechanisms under such multiaxial loading. This study addresses this critical research gap by investigating, for the first time, the consolidation behavior and mechanical response of CPB subjected to realistic, time-dependent multiaxial stress paths under both drained and undrained curing conditions. Utilizing a novel CPB curing and monitoring apparatus, this study will simulate these complex curing conditions to provide new insights into how CPB consolidates in response to the challenging stress environments typical of deep mining operations. This research is not only original in its approach but also crucial for improving the safety and efficiency of backfilling practices, ultimately contributing to the stability and sustainability of underground mining activities.

2. Experimental program

2.1. Multiaxial compressive stresses curing and monitoring apparatus

To simulate various rockwall closure scenarios, we utilized an innovative multiaxial compressive stress curing and monitoring apparatus, depicted in Fig. 2, developed at the University of Ottawa (Liu and Fall, 2024). The comprehensive design and operational features of this apparatus are detailed in Liu and Fall (2024).

The apparatus consists of five independent loading actuators, each equipped with a load cell and a linear variable differential transformer (LVDT) for accurately measure applied stress and corresponding deformations of the CPB sample. Compressive stress can be applied along multiple axes ($\sigma_{-z} = \sigma_z, \sigma_{-x} = \sigma_x = \sigma_{-y} = \sigma_y$), where σ_x and σ_y present the horizontal stresses due to rockwall closure, and σ_z simulates vertical stress from the self-weight of the CPB and any overlying strata. Multiaxial stresses were applied by operating the actuators to drive loading pistons in a controlled load path. Each actuator can apply stress up to 6 MPa, allowing for flexible simulation of various in situ stress conditions observed in deep mining environments. A customized sample cell was precisely centered within a sealed chamber, designed to withstand the multiaxial loading from the five loading pistons. Data acquisition is facilitated through a seamless connection to a computer system, enabling comprehensive record-keeping and subsequent analysis. Additionally, the apparatus provides precise control over drainage conditions during the curing process, allowing for simulations under both drained and undrained scenarios. The sample cell bottom plate incorporates a drainage control system consisting of a seepage stone, a drainage path, and a drainage valve. For undrained conditions, the CPB sample was completely encapsulated in sealed rubber membrane (internal dimensions matching the sample: 160 mm × 54 mm × 54 mm; membrane thickness: 1 mm), and the drainage value was kept closed to prevent fluid escape. For drained conditions, the CPB sample was enclosed with a rubber membrane featuring a circular opening on the bottom side, precisely aligned with the seepage stone. In this configuration, the drainage valve was opened and connected to a collection bottle via tubing to collect expelled water during curing.

Prior to use, every load and displacement channel was calibrated according to ASTM E4-24 standard. Vertical and horizontal load cells were verified up to 60 kN with a NIST-traceable digital force calibrator (accuracy ±0.5 % F.S.), and each axial LVDT was calibrated with a digital micrometer (±0.002 mm). Linearity tests at 20 %, 50 % and 90 % of span yielded $R^2 \geq 0.999$. To quantify possible frame- or platen-compliance, a 54 × 54 × 160 mm steel prism ($E = 200$ GPa) was loaded to 6 MPa, in 0.5 MPa increments, along each axis simultaneously. The theoretical elastic shortening of the steel bar under 6 MPa (horizontal direction, gauge = 54 mm) is 0.00162 mm. The in-frame LVDTs recorded a total displacement of 0.004 mm in horizontal axis; the residual attributable to frame + platen compliance is therefore 0.000238 mm. This is one order of magnitude smaller than the minimum deformation increment reported in this study. Thus, the frame deflection has a negligible influence on measured deformation over the stress range investigated.

As with most multiaxial stress-application systems, the present apparatus has minimal experimental limitations. Specifically, slight friction may occur between the sidewalls and the cell frame during stress application, which could introduce insignificant nonuniformities in the stress distribution. To minimize this effect, a thin layer of silicone-based lubricant was applied between the

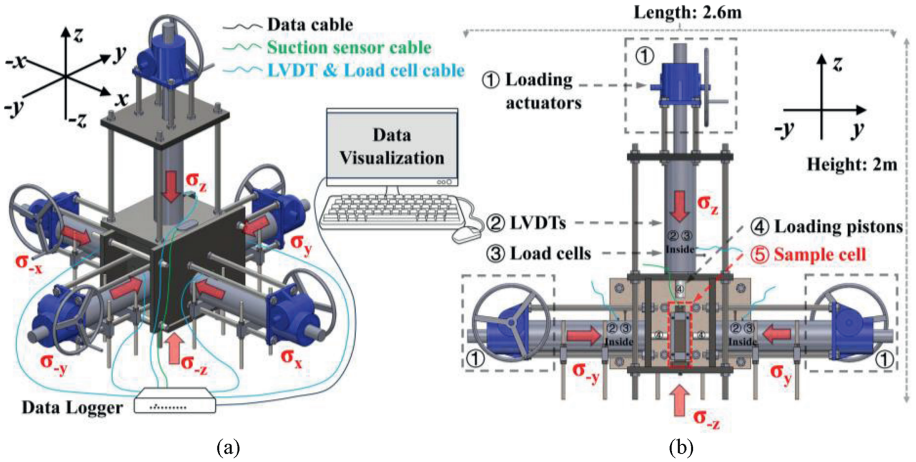

Fig. 2. Schematic diagram of the multiaxial compressive stress curing and monitoring apparatus: (a) Isometric view, and (b) Cutaway view.

sidewalls and the frame prior to specimen preparation. In addition, axial displacements were continuously monitored using multiple LVDTs along different directions to detect any potential asymmetric deformation during curing. These mitigation measures effectively reduce the influence of sidewall friction, and the observed consolidation behavior and mechanical property development trends remain reliable and representative of CPB behavior under field-relevant conditions.

2.2. Materials

Synthetic silica tailings (ST) were selected for preparing the CPB mixtures instead of natural tailings to eliminate the variability introduced by unknown chemical constituents that could interfere with cement hydration and compromise reproducibility. The ST used in this study exhibit a high purity level (99.8 % silicon dioxide (SiO_2)) and consistent physical properties, providing a controlled and repeatable experimental environment. Table 1 presents the physical characteristics of ST. Additionally, the particle size distribution (PSD) of the ST, as shown in Fig. 3, closely matches that of natural tailings from nine different mines in Canada, supporting the relevance of ST as a representative substitute in laboratory research. Tap water was used as the mixing water to better reflect practical field conditions, where tap water is commonly employed in CPB production rather than deionized water. The use of tap water also avoids introducing unknown chemical constituents that may be present in process water recovered from tailings treatment circuits. This choice ensures that the experimental results maintain practical applicability while preserving sufficient quality control and consistency for laboratory testing. General use (GU) Portland cement was selected as the binder, with its properties listed in Table 2.

2.3. Sample preparation and mix proportions

Table 3 provides a full description of the CPB mixtures used in this study. Following the listed mix proportions, GU Portland cement, ST, and tap water were mixed for 10 min in a concrete mixer. After the mixing process, the fresh CPB paste was poured into the customized sample cell inside the apparatus and subjected to different curing conditions (Table 3) using the previously described multiaxial compressive stress curing and monitoring apparatus (Liu and Fall, 2024). The workability of the fresh CPB mixtures was evaluated using a slump test in accordance with ASTM C143 (2010), resulting in a slump measurement of 18 cm, which is a suitable value for CPB applications.

During the curing process, three distinct stress conditions were simulated. The first condition involved no stress, serving as a stress-free baseline for comparison. The second condition, termed Multiaxial Compressive Stress Condition 1 (MCS1), applied a specific combination of vertical and horizontal stresses corresponding to rockwall closure scenario 1. The third condition, Multiaxial Compressive Stress Condition 2 (MCS2), utilized a different combination of vertical and horizontal stresses to assess the impacts of varying rockwall closure scenarios, with the development of these rockwall closures detailed in Section 2.4. In addition, all samples were maintained at a consistent curing temperature of 20 °C to ensure controlled environmental conditions.

Table 1
Physical properties of the silica tailings (ST).

Element	G_s	D_{10} (μm)	D_{30} (μm)	D_{50} (μm)	D_{60} (μm)
ST	2.7	1.9	9	22.5	31.5

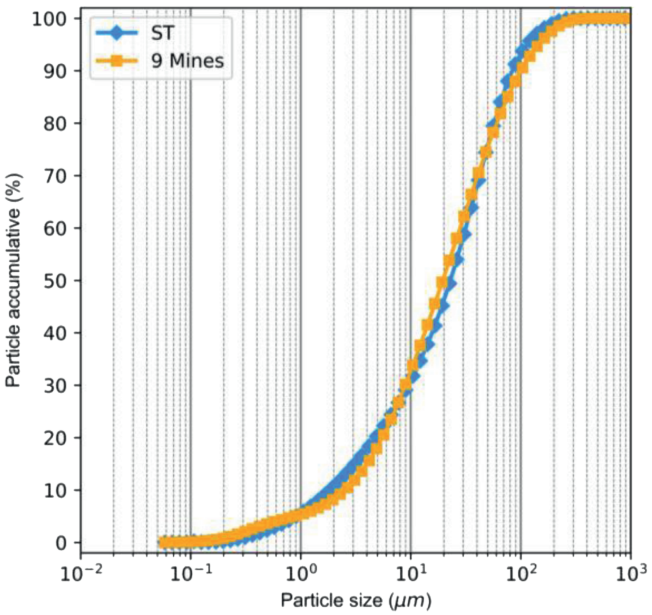

Fig. 3. Particle size distribution (PSD) of the silica tailings and average PSD of tailings from nine different mines in Canada.

For each stress condition, CPB samples were cured under both drained and undrained scenarios to examine the influence of drainage on consolidation behavior and mechanical properties. In conventional consolidation testing (e.g. ASTM D2435), "drained" and "undrained" conditions refer to the ability of water to move vertically through porous stones placed at the top and bottom of a specimen under vertical loading. In contrast, our curing-based consolidation tests were conducted under multiaxial stress paths with drainage control implemented through the bottom of the sample cell. In the drained condition, the bottom drainage path was open and connected to a collection system, allowing excess water expelled during CPB curing to escape freely. In the undrained condition, the sample was completely enclosed in a sealed rubber membrane and the drainage valve was closed, preventing water movement out of the specimen. These definitions differ from conventional methods but are appropriate for simulating the hydraulic boundary conditions encountered during underground backfilling, where CPB may be in contact with permeable or impermeable boundaries. This setup allows for a realistic examination of how drainage availability affects consolidation, strength gain, and mechanical performance of CPB under field-relevant stress conditions.

To facilitate clear identification, CPB samples subjected to multiaxial compressive stresses are labeled as MCS-CPB. For instance, a sample designated as MCS1-UD-CPB refers to a CPB specimen exposed to the multiaxial compressive stress condition (MCS1) under undrained conditions (UD). Here, MCS signifies the application of both vertical stresses (originating from self-weight) and two horizontal stresses induced by rockwall closure.

2.4. Multiaxial compressive stress curing conditions

Fig. 4 illustrates the targeted in situ stress profiles, represented by dash lines, alongside the stresses applied during the curing simulation process, depicted as solid lines. In this study, both MCS1 and MCS2 conditions employed an identical vertical stress curve (blue curve in Fig. 4) to replicate a uniform backfilling operation. This operation proceeded at a filling rate of 0.31 m/h,

Table 2
Characteristic of general use (GU) Portland cement.

Type of binder	MgO (%)	CaO (%)	SiO_2 (%)	Al_2O_3 (%)	Fe_2O_3 (%)	SO_3 (%)	Relative density	Specific surface (m^2/g)
GU	2.65	62.82	18.03	4.53	2.7	3.82	3.1	1.3

Table 3
Curing conditions, mix proportions, and curing time of the CPBs.

Sample designation	Curing conditions		Mix proportions		Curing time (d)
	Stress Cond. [a]	Drainage	Binder (%) [b]	Con. Ratio (%) [c]	
Control-UD-CPB	Stress-free	Undrained	7	74	1, 3, 7, 28
MCS1-UD-CPB	MCS1	Undrained			
MCS2-UD-CPB	MCS2	Undrained			
Control-D-CPB	Stress-free	Drained			
MCS1-D-CPB	MCS1	Drained			
MCS2-D-CPB	MCS2	Drained			

[a] Stress Condition (Stress Cond.): "MCS" denotes multiaxial compressive stress condition. MCS1 and MCS2 refer to specific stress conditions detailed in section 2.4.
[b] Binder: GU Portland cement was used as the binder, constituting a specified percentage of the total mass of fresh CPB.
[c] Concentration Ratio (Con. Ratio): The solid mass (GU and ST) divided by the total mass of the CPB mixture.

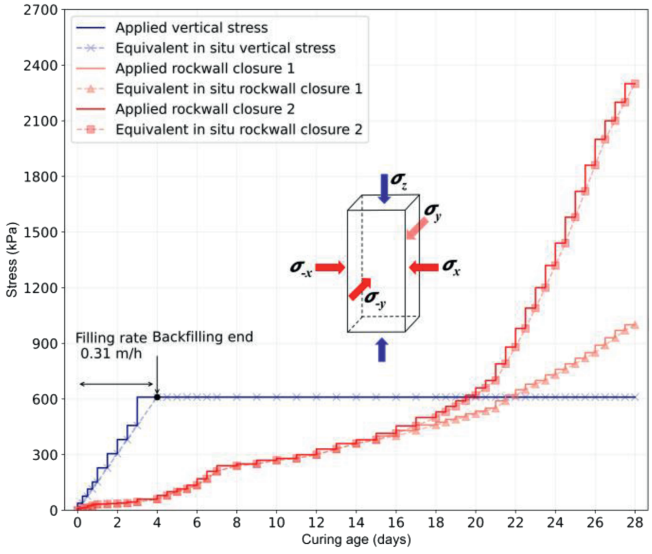

Fig. 4. Application of vertical stress and horizontal stresses simulating various rockwall closure scenarios.

ultimately achieving a backfill height of 29.76 m (vertical stress of 610.08 kPa). This approach reliably replicates the self-weight effect of the CPB mass in field conditions. It is acknowledged that in many mining operations, backfilling is implemented in batches rather than as a continuous process. However, in deep mines, continuous backfilling offers significant advantages, including improved transport efficiency, reduced risks of pipeline blockage due to early cement hydration, and enhanced operational stability. Continuous filling at a steady rate, as simulated in this study, better replicates ideal operational conditions aimed at minimizing transportation risks and ensuring uniform stress development. Accordingly, this study adopts a continuous backfilling scenario to improve the practical transferability of the findings to deep mining operations where continuous filling is increasingly preferred.

The key differentiation between MCS1 and MCS2 conditions lies in the manner of horizontal stress development induced by rockwall closures. The design of the horizontal stress loading paths for rockwall closure scenarios 1 and 2 was based on field observations reported in previous studies (Hassani et al., 1998; Williams et al., 2001; Thompson et al., 2009; Seymour et al., 2017; Raffaldi et al., 2019). In particular, Raffaldi et al. (2019) provided detailed in situ measurements of stope closure and backfill-induced stresses at the Lucky Friday mine, which were used as a benchmark reference in previous work by Liu and Fall (2024). Rockwall closures 1 and 2 were formulated to represent lower-intensity and more gradual closure rates relative to the extreme closure observed in certain deep mines, reflecting more typical conditions encountered across a broad range of underground operations. During the first 14 d of curing, the applied horizontal stresses were kept low and increased steadily, consistent with field observations where early closure rates and stress magnitudes are generally low (below 400 kPa) during the initial backfill consolidation period. After this phase, stress escalation was introduced at varying rates to simulate progressive mining-induced deformation. This design ensures that the applied stress magnitudes and loading rates are representative of real-world backfilling conditions in deep mines. For each rockwall closure scenario, the horizontal stresses ($\sigma_x = \sigma_{-x} = \sigma_y = \sigma_{-y}$) were meticulously controlled to advance at consistent rates.

It is acknowledged that the rheological properties of the surrounding rock mass, such as creep and stress relaxation, can significantly influence the time-dependent development of rockwall closure stresses acting on CPB. Previous studies, such as the recent work by Geng et al. (2024) on secondary support optimization under high in situ stress conditions, have emphasized the critical role of rock rheology in long-term deformation and support behavior. In this study, however, the focus was placed on replicating the field-measured stress conditions experienced by CPB, rather than explicitly modeling the surrounding rock behavior. Therefore, while the applied stress paths inherently reflect the combined effects of rock mass rheology and mining activities observed in the field, the rheological properties of the surrounding rock were not independently analyzed. Future work could further explore the direct coupling between CPB performance and the time-dependent mechanical behavior of the host rock mass to improve the mechanistic understanding of stope-scale consolidation and long-term backfill stability.

2.5. Testing method

2.5.1. Mechanical tests

At designated curing ages of 1, 3, 7, and 28 d, CPB samples were retrieved from the customized sample cell and then cut into dimensions of 50 mm × 50 mm × 50 mm. The unconfined

compressive strength (UCS) of these specimens was evaluated in accordance with ASTM C109 standard. Testing was conducted using a compression machine with a maximum capacity of 50 kN, applying a load rate of 1 mm/min. Each UCS measurement was performed in duplicate, and the average value was reported as the definitive UCS for each sample.

2.5.2. Physical properties tests

The physical characteristics of the specimens were evaluated based on key parameters, including dry density (ρ_d), porosity (n), and gravimetric water content (w). After the curing process, samples were carefully extracted from the curing cell. The dimensions of each sample were measured using a digital caliper. Subsequently, the mass of each specimen was measured using a precision electronic balance. The samples were then subjected to desiccation in a thermostatically controlled drying oven at a constant temperature of 45 °C for a minimum duration of 4 d to ensure the complete removal of free water. The dry mass was recorded, and the values of w and ρ_d were calculated based on the changes in mass and the initial specimen volume. Specific gravity (G_s) measurements were performed on approximately 50 g of finely ground oven-dried CPB material, following the procedure described in ASTM D854-14 using a pycnometer. Based on the measured dry density (ρ_d) and specific gravity (G_s), the porosity (n) was calculated using the relation of $1 - \rho_d/(G_s\rho_w)$, where ρ_w is the density of water. These tests were conducted using conventional geotechnical laboratory equipment, following standardized ASTM procedures, to ensure accuracy and consistency in characterizing the physical properties of the CPB specimens under the specific experimental conditions.

2.5.3. Monitoring of multiaxial deformations

Multiaxial deformations experienced by the CPB under compressive loading were continuously monitored using LVDTs installed along each stress axis, as illustrated in Fig. 2. These sensors provided real-time data on the dimensional changes of the CPB samples, enabling precise tracking of deformation behaviors under varying stress conditions. They allow accurate and synchronized measurement of deformations across all applied stress directions.

3. Results and discussion

3.1. Consolidation behaviour under multiaxial stress loading conditions

Fig. 5 illustrates the evolution of the normalized void ratio of CPB cured under different multiaxial (3D) stress conditions for both drained and undrained conditions. Additionally, two x-axes are plotted on the top, displaying the magnitudes of the horizontal stress (σ_H, where $\sigma_{-x} = \sigma_x = \sigma_{-y} = \sigma_y$) and vertical stress ($\sigma_V$, where $\sigma_{-z} = \sigma_z$), corresponding to specific curing ages indicated by the tick values on the bottom x-axis. This visualization arrangement is applied across all subsequent figures to allow readers to quickly reference the corresponding curing stress conditions. The normalized void ratio was calculated based on the monitored deformation (volume change) of CPB and its initial volume. This figure shows that the multiaxial stress application for both MCS1 and MCS2 was identical during the initial 14-d period. Given this similar curing condition during this period, the normalized void ratios of samples under MCS1 and MCS2 conditions were expected to be identical during this time for both drained and undrained conditions. After the 14th day, all samples exhibited different values due to varying curing conditions (stress magnitude and drainage conditions). The results also indicated that the normalized void ratio of drained samples consistently remained lower than that of undrained samples under multiaxial stress, suggesting that drained samples generally underwent deformation more rapidly. The mechanisms responsible for this behaviour are discussed below.

Fig. 5 further illustrates that the magnitude and rate of decrease in the normalized void ratio (indicating the reduction in backfill volume) are not constant over time and during stress application. Instead, the process exhibits distinct stages or phases, each characterized by different magnitudes or rates of volume reduction. Within the first 24 h, both undrained (MCS1-UD-CPB) and drained (MCS1-D-CPB) samples exhibited a significant drop in their normalized void ratio, indicating rapid volume reduction. Specifically, the normalized void ratio of MCS1-UD-CPB samples decreased from 1 to 0.970, while that of MCS1-D-CPB samples dropped more sharply from 1 to 0.943. During this period, horizontal stress increased from 0 kPa to 32 kPa, and vertical stress rose from 0 kPa to 152 kPa (Fig. 4). Despite the absence of drainage, the initial rapid compression of the undrained CPB demonstrated the high compressibility of fresh undrained CPB under multiaxial stress. In contrast, the presence of drainage in drained CPB (MCS1-D-CPB) facilitated pore water expulsion, leading to greater volume reduction and resulting in a lower normalized void ratio in the drained samples.

During the subsequent 3-d period (Days 1–4), the rate of decrease in normalized void ratio slowed regardless of drainage conditions. This means that the consolidation in MCS-CPBs (MCS1-UD-CPB and MCS1-D-CPB) proceeded at a more gradual pace compared to the initial 24 h of curing, despite the applied stresses increasing significantly during the 1st to 4th day period: horizontal stress increased from 32 kPa to 60 kPa and vertical stress from 152 kPa to 610 kPa. This can be attributed to the strengthening effect of cement hydration during early ages (Junior et al., 2012; Ghirian and Fall, 2016; Cui and Fall, 2016; Hou et al., 2018), which enhances resistance against compression under the applied multiaxial stress.

While the initial stages of curing were dominated by rapid consolidation and compression, the influence of stress magnitude and drainage conditions became increasingly complex as curing progressed. Between the 4th and 14th day of curing, the rate of decrease in normalized void ratio (i.e. the rate of consolidation) further slowed for undrained samples (MCS1-UD-CPB), with values decreasing from 0.944 to 0.918. In contrast, the drained samples (MCS1-D-CPB) maintained a more moderate decrease, with the ratio dropping from 0.925 to 0.883. During this period, vertical stress remained constant at 610 kPa, reflecting the end of the backfilling process, while horizontal stress increased from 60 kPa to 360 kPa, indicating higher rockwall closure stress. The moderate rate of consolidation in drained samples can be attributed to the continued expulsion of pore water. Conversely, the undrained samples, unable to drain water, initially experienced self-desiccation as the cement hydrated and consumed a portion of the pore water (Grabinsky et al., 2006; Li and Fall, 2016; Wang et al., 2016), leading to a lower rate of water loss compared to the drained samples, supported by the gravimetric water content results in Fig. 6. This lower water loss explains the reduced consolidation magnitude and rate in the undrained samples. Furthermore, as compression continued from the 4th to the 14th day, the remaining pore water in the undrained samples was subjected to increasing pressure, likely causing a buildup of pore water pressure. This pressure buildup provided additional resistance to further compression, contributing to the slower reduction in the normalized void ratio compared to the drained samples.

After 14 d, the normalized void ratio once again decreased at a fast rate for undrained samples under the MCS1 condition, which

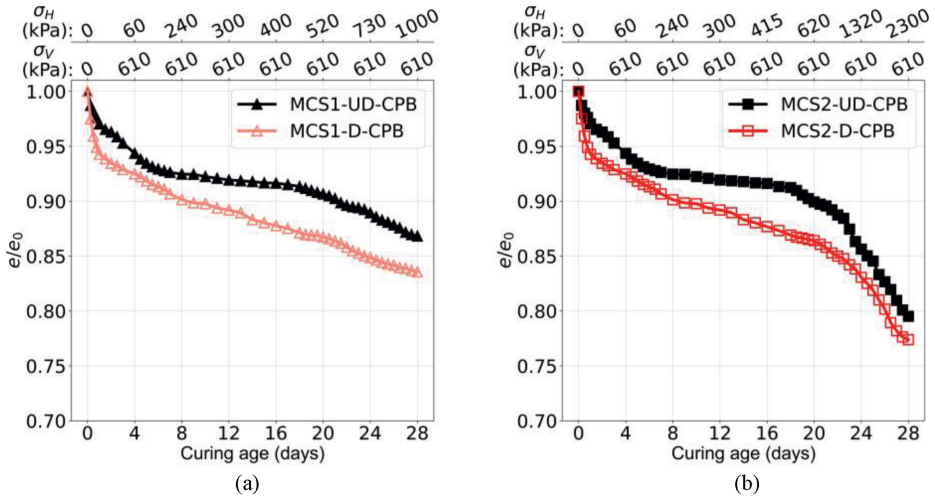

Fig. 5. Evolution of normalized void ratio of CPB cured under multiaxial stress loading for undrained and drained conditions: (a) MCS1-CPB, and (b) MCS2-CPB.

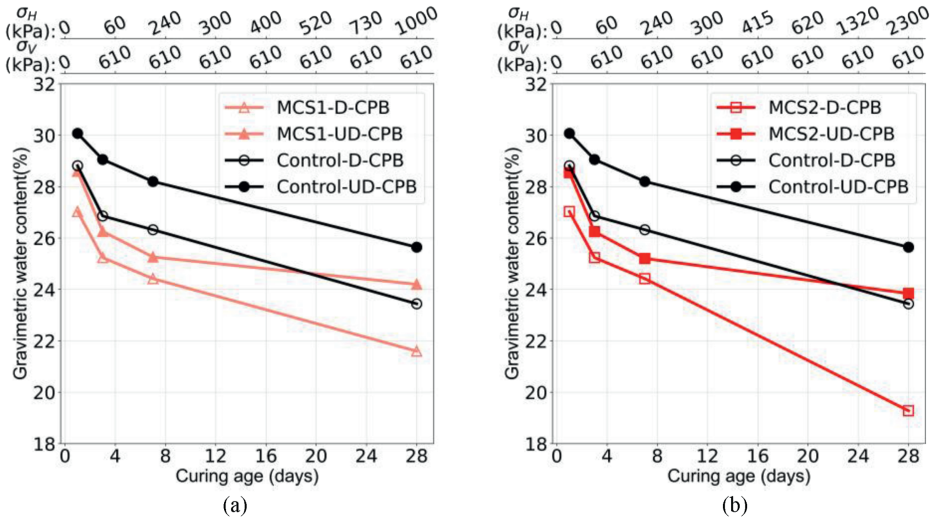

Fig. 6. Evolution of gravimetric water content of CPB cured under multiaxial stress loadings for undrained and drained conditions: (a) MCS1-CPB, and (b) MCS2-CPB.

even caught up with the decreasing rate for drained samples. For undrained samples, the ratio decreased from 0.918 to 0.868, representing a reduction of 0.050. In the drained samples, the ratio decreased from 0.883 to 0.836, with a reduction of 0.047. During this period, the horizontal stress (induced by rockwall closure) nearly tripled, rising from 360 kPa to 1000 kPa, while the vertical stress (corresponding to the height of the backfill mass) remained constant at 610 kPa. These higher horizontal stresses intensified the compression of the MCS samples, pushing the particles closer together and further enhancing cement hydration (Liu and Fall, 2024), which consumed more pore water during days 14–28 than the Control samples. This led to more chemical shrinkage from cement hydration and a greater reduction in void space in MCS samples (Muir Wood and Doherty, 2014; Qin et al., 2021; Yang et al., 2021). The observed increase in dry density in the CPB samples over the curing period, as illustrated in Fig. 7, confirms that elevated induced horizontal stresses compact the particles more closely together. Specifically, this figure reveals a significant rise in the dry density of the MCS1 samples during the period when horizontal stress increased from 360 kPa to 1000 kPa. The drained samples, having developed increased stiffness due to faster consolidation during the 0–14 d period, were better able to resist further compression during the 14–28 d period, even as the multiaxial stress increased. This enhanced stiffness occurred because the initial consolidation had expelled much of the pore water, allowing the particles to become more tightly packed. This is evidenced by the higher dry density observed in MCS1-D-CPB samples. For instance, after 7 d of curing, the dry density of MCS1-D-CPB reached 1.502 g/cm^3, compared to the Control-D-CPB's dry density of 1.463 g/cm^3. As a result, the material became more compact and less prone to deformation. Consequently, the rate of consolidation slowed slightly during the 14–28 d period, as the CPB had already undergone significant compaction and further compression required much higher stress levels to induce additional deformation.

Under the MCS2 condition, i.e. higher magnitude of rockwall closure stress, where horizontal stress increased dramatically from 360 kPa to 2300 kPa while vertical stress remained constant at 610 kPa, both drained and undrained samples exhibited significantly greater rates of consolidation and compression compared to MCS1 samples. The normalized void ratio of MCS2-UD-CPB decreased from 0.918 at the 14th day to 0.795 at 28th day, while

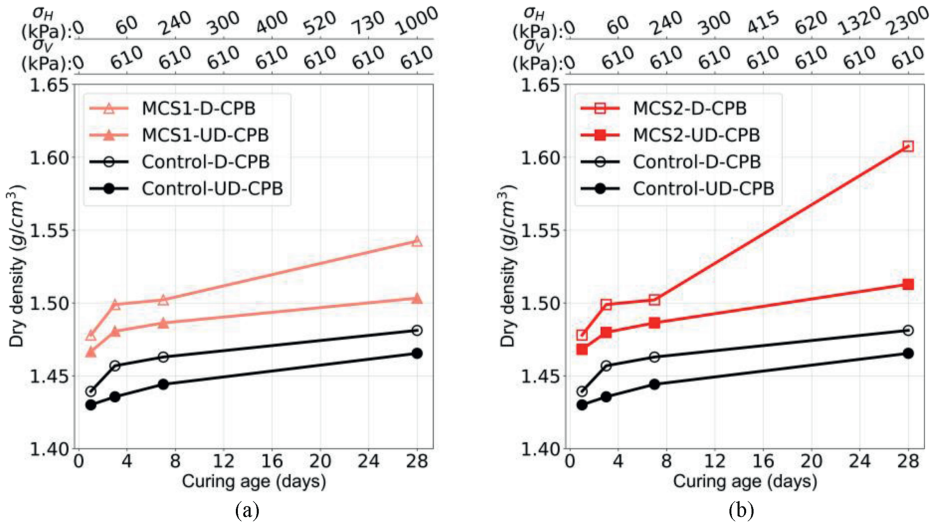

Fig. 7. Development of dry density of CPB cured under multiaxial stress loadings for undrained and drained conditions: (a) MCS1-CPB, and (b) MCS2-CPB.

MCS2-D-CPB decreased from 0.883 to 0.774. The higher and rapidly increasing horizontal stress, indicative of stronger and faster rockwall closure, significantly enhanced consolidation in drained samples (MCS2-D-CPB). The elevated horizontal stress was sufficient to overcome the increased resistance of MCS2-D-CPB sourced from the improved cement hydration during the 0–14 d period. Additionally, it drove undrained samples (MCS2-UD-CPB) into a new state with a more favorable pore structure for hydration reactions (Zhou and Beaudoin, 2003; Liu and Fall, 2024), leading to more effective chemical shrinkage. The faster consumption of pore water by hydration reaction would prevent the buildup of positive pore water pressure despite the decreasing void space (Doherty, 2015; Ghirian and Fall, 2016; Jaouhar and Li, 2019; Al-Moselly and Fall, 2024b), allowing for more effective compression at the later curing stages.

When comparing the effect of drainage on the consolidation and compression between MCS1 and MCS2 conditions, the difference in normalized void ratio between MCS2-UD-CPB and MCS2-D-CPB on the 28th day, was 0.021, which is lower than the difference of 0.032 observed under MCS1 conditions. This reduction indicates that higher rockwall closure stress levels, as seen in MCS2, reduced the impact of the drainage on the consolidation behavior of CPB, suggesting that under extreme stress conditions, often encountered in deep mines, the difference between drained and undrained behavior became less pronounced at later curing stages.

3.2. Impact of consolidation behavior under multiaxial stress loading on the UCS development of CPB

The consolidation behavior of CPB critically influences its strength development by enhancing particle compaction, affecting effective stress, and accelerating hydration reactions (Cui and Fall, 2017a). Fig. 8 illustrates the evolution of UCS of CPB under different multiaxial stress (rockwall closure) loadings for both undrained and drained conditions. Additionally, Fig. 9 shows the strength contribution from the application of multiaxial curing stress under both undrained and drained conditions, which was calculated from the UCS of CPB under multiaxial stress divided by the UCS of control samples.

Fig. 8 shows that the UCS of CPB under multiaxial curing stress conditions consistently surpasses that of CPB cured under control conditions (stress-free curing conditions) at all curing ages, irrespective of the drainage or consolidation conditions. After just one day of curing, the benefits of multiaxial stress are already evident. Under undrained conditions, the UCS (0.729 MPa) of MCS1-UD-CPB was significantly higher than that (0.559 MPa) of Control-UD-CPB, representing a 30.4 % increase (Fig. 9). In drained samples, MCS1-D-CPB achieved 0.972 MPa compared to 0.678 MPa for Control-D-CPB, showing a greater increase of 43.3 %. As curing progressed, the multiaxial stress loadings continued to enhance the compressive strength of CPB in both drained and undrained conditions. Between the 14th and 28th days, the horizontal stress in MCS1 condition nearly tripled, increasing from 360 kPa to 1000 kPa, while vertical stress remained constant at 610 kPa. Under these conditions, the UCS of drained samples (MCS1-D-CPB) reached 3.007 MPa by the 28th day, representing a 21.3 % increase compared to Control-D-CPB (2.478 MPa). Similarly, undrained samples (MCS1-UD-CPB) exhibited a UCS of 2.563 MPa, a 12.6 % increase over the 2.276 MPa observed in Control-UD-CPB. These results suggest that the application of multiaxial curing stress, whether in drained or undrained conditions, positively influences the strength development in CPB. This significant improvement can be attributed to the pronounced influence of multiaxial compressive stresses, which promote pore structure refinement and densification in the CPB while enhancing cement hydration, particularly during the initial stages of curing. At these initial curing ages, the CPB undergoes the hardening process. The rapid application of vertical stress, resulting from the backfilling of the mine cavity at a rate of 0.31 m/h, aids in particle settling, while the progressively increasing horizontal stresses from four distinct directions due to rockwall closure facilitates further densification of the MCS-CPB. These dynamic stresses work synergistically to reduce void spaces, as shown in Fig. 10. Fig. 10 presents the porosity results for both the control samples and the samples subjected to multiaxial curing stresses (MCS1-CPB and MCS2-CPB). The porosity data presented in Fig. 10 consistently demonstrate that the “empty" space within MCS-CPB is significantly less than that in the Control-CPB across all curing ages. Notably, at 28 d of curing, MCS2-CPB, which experiences greater horizontal rockwall closure stress, shows a significant reduction in porosity compared to Control-CPB. Specifically, under undrained conditions, the porosity of MCS2-CPB is reduced by 5.68 %, while under drained conditions, the reduction is an impressive 11.53 %. In

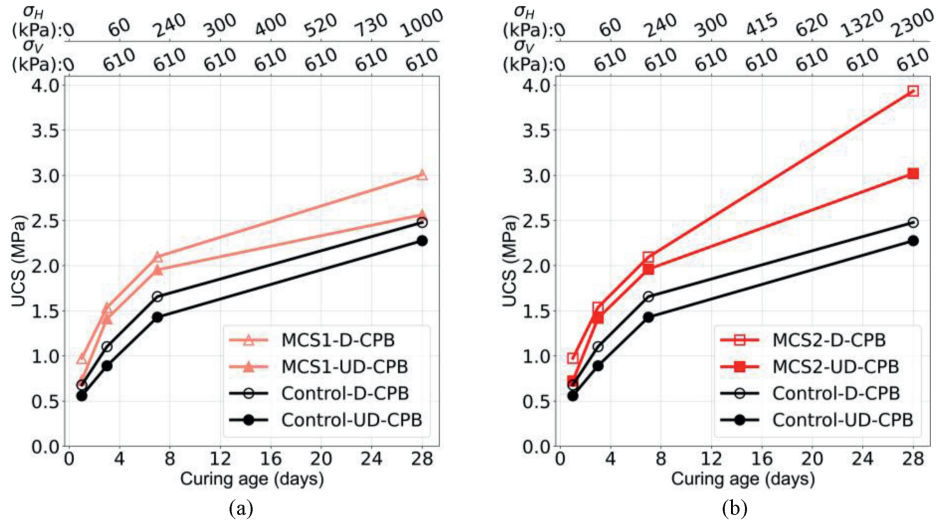

Fig. 8. Strength development of CPB cured under multiaxial stress loadings for undrained and drained conditions: (a) MCS1-CPB, and (b) MCS2-CPB.

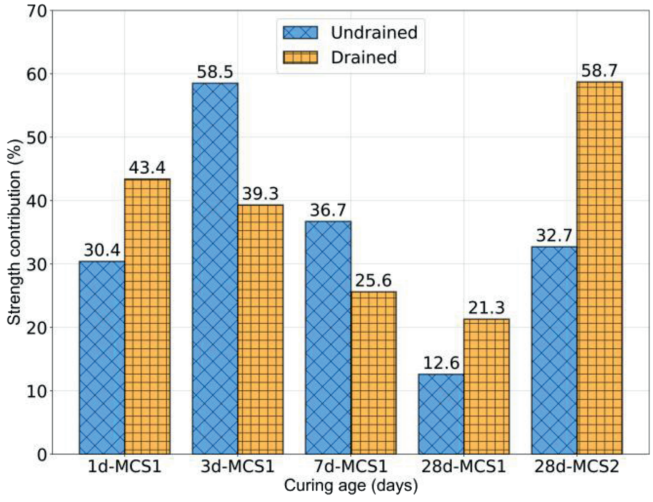

Fig. 9. Strength contribution of multiaxial stress in drained and undrained conditions.

contrast, MCS1-CPB exhibits smaller reductions of 3.81 % and 5.75 %, respectively. These findings underscore the substantial impact of increased horizontal stress in MCS2, which leads to a greater compaction of void spaces. Furthermore, previous research (e.g. Liu and Fall, 2024) has shown that multiaxial compressive curing stresses accelerate cement hydration in CPB systems during the early stages of curing (0–7 d). This accelerated hydration results in the production of a greater quantity of cement hydration products, thereby enhancing the strength of backfill materials cured under these conditions. Evidence of this enhanced hydration is provided by the gravimetric water content analysis conducted on CPB samples cured under multiaxial compressive stresses compared to control samples, as illustrated in Fig. 6. The results indicate that MCS-CPB samples exhibit lower water content and a faster rate of water content reduction, particularly within the first 7 d. This suggests more pronounced self-desiccation, caused by water consumption during cement hydration, in MCS-CPB samples compared to the controls. In other words, cement hydration occurs more rapidly in samples subjected to multiaxial compressive

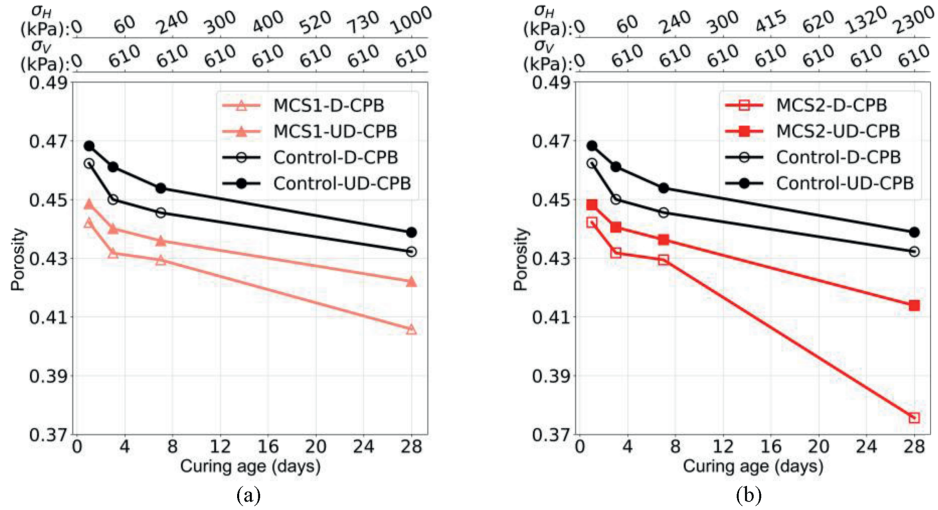

Fig. 10. Evolution of porosity of CPB cured under multiaxial stress loadings for undrained and drained conditions: (a) MCS1-CPB, and (b) MCS2-CPB.

stress conditions. These findings align with those of Zhou and Beaudoin (2003), who reported that applying a curing pressure of 6.80 MPa during the early stages of Portland cement hydration significantly increases the degree of hydration and results in a denser microstructure within 48 h. Similarly, Ghirian and Fall (2015) demonstrated the substantial impact of curing stresses on cement hydration in backfill systems. Their study showed that CPB samples subjected to stress during curing exhibited greater formation of hydration products such as C-S-H and CH compared to samples cured under stress-free conditions. This highlights the critical role of curing stresses in promoting hydration reactions and improving the microstructure of CPB materials.

Moreover, the analysis of the results presented in Figs. 8 and 9, as described earlier, indicates that under multiaxial stress curing conditions, CPBs cured in drained conditions consistently exhibit a greater increase in UCS compared to those cured in undrained conditions. This indicates that multiaxial stress had a greater impact on strength improvement in drained conditions. For example, after just one day of curing, drained samples (MCS1-D-CPB) exhibited a 43.3 % improvement in UCS compared to Control-D-CPB, whereas undrained samples (MCS1-UD-CPB) showed a 30.4 % improvement over Control-UD-CPB (Fig. 9). This behavior can be attributed to the greater degree of consolidation experienced by CPBs cured under drained conditions, as evidenced by Fig. 5. Enhanced consolidation leads to a more refined pore structure, as illustrated in Fig. 7, which in turn contributes to the increased strength of the CPB. In drained conditions, the dissipation of pore water pressure occurs through a combination of water drainage and water consumption during cement hydration (self-desiccation). In contrast, for CPBs cured under undrained conditions, pore water pressure dissipation relies solely on the self-desiccation process. This difference underscores the critical role of drainage in facilitating more effective consolidation and strengthening the CPB structure, even under multiaxial compressive curing stress conditions.

In addition, the analysis of Figs. 8 and 9 reveals that the magnitude and rate of increase of horizontal stress induced by rockwall closure significantly influence UCS development, regardless of whether the CPB is cured under undrained or drained conditions. As shown in Fig. 4, starting from 14 d of curing, the horizontal stress applied to the CPB samples began to diverge notably between MCS1 and MCS2 conditions. Between the 14th and 28th days, horizontal stress in MCS1 increased from 360 kPa to 1000 kPa while vertical stress remained constant at 610 kPa (indicating a constant backfill structure height). In contrast, under MCS2 conditions, horizontal stress increased dramatically from 360 kPa to 2300 kPa, while the vertical stress similarly remained constant at 610 kPa. Fig. 8 shows that, irrespective of drainage conditions, the 28-d UCS of MCS2-CPB was significantly higher (15 %–30 %) than that of MCS1 samples. For instance, in undrained conditions, the UCS of MCS2-UD-CPB reached 3.02 MPa on the 28th day, representing a 32.7 % increase compared to 2.276 MPa observed in Control-UD-CPB (Figs. 8 and 9). This 32.7 % increase under MCS2 conditions far exceeds the 12.6 % increase observed under MCS1 conditions for undrained samples (Fig. 9). These results indicate that even without drainage, the higher and more rapidly increasing rockwall closure stress in MCS2 conditions, combined with the self-weight loading of CPB, significantly enhanced the material's strength. In drained conditions, the effect of the magnitude and rate of increase of horizontal stress induced by rockwall closure was even more pronounced. The UCS of MCS2-D-CPB on the 28th day reached 3.933 MPa, markedly higher than the 2.478 MPa observed for Control-D-CPB, representing a 58.7 % increase. This increase under MCS2 conditions was also significantly greater than the 21.3 % increase observed under MCS1 conditions for drained samples (Fig. 9). The superior UCS values observed in MCS2 samples, whether cured in undrained or drained conditions, are primarily attributed to the higher and more rapidly developing horizontal stress, indicative of stronger and faster rockwall closure. This increased stress significantly enhanced the compression and consolidation of CPB samples. These effects were particularly pronounced in drained samples (MCS2-D-CPB), where consolidation was much more effective compared to undrained samples (MCS2-UD-CPB), as discussed earlier. In undrained samples, pore water pressure dissipation or consolidation occurs solely through self-desiccation, while drained samples benefit from both water drainage and self-desiccation. These synergistic compression and consolidation processes led to greater void space reduction (Figs. 5 and 10) and higher dry density (Fig. 7) in samples subjected to higher and more rapidly increasing horizontal stress, especially in drained conditions. The refinement of the CPB pore structure resulting from these processes is closely associated with the observed increase in UCS.

Furthermore, Fig. 8 illustrates that the UCS of CPB increases with curing time, characterized by rapid early-age strength development followed by slower growth at later stages. This trend is consistent across both drained and undrained conditions under multiaxial stress and stress-free conditions. During the first three days, the UCS of CPB increases sharply. For instance, the UCS of MCS1-D-CPB rises from 0.972 MPa on the first day to 1.536 MPa by the third day, representing a 58 % increase. Similarly, MCS1-UD-CPB exhibits a 93.7 % increase over the same period. This significant early-age strength gain is attributed to the combined effects of accelerated cement hydration and a higher rate of consolidation. The faster rate of consolidation observed in CPB subjected to multiaxial compressive stresses during the first 3 d is evident in Fig. 5. However, after the first 3 d, the rate of strength increase slows, coinciding with a deceleration in consolidation in the MCS samples (Fig. 5). Between the 3rd and 7th days, the UCS of MCS1-D-CPB increases by 36.6 %, while MCS1-UD-CPB shows a 38.4 % increase. This reduced growth rate is typical as hydration slows, the consolidation process decelerates, and the CPB pore structure stabilizes. By the 28th day, the growth rate slows even further, with the UCS of MCS1-D-CPB showing only a 43.3 % increase over the curing period from the 7th to the 28th day.

Additionally, as curing continued, a delayed strength contribution from multiaxial stress became apparent in undrained samples. This is reflected in the fact that the strength contribution from multiaxial stress for undrained samples surpassed that for drained samples. By 3 d of curing, UCS improvement for undrained samples (MCS1-UD-CPB) reached 58.5 % compared to Control-UD-CPB, while the improvement for drained samples (MCS1-D-CPB) was 39.3 % compared to Control-D-CPB (Fig. 9). This trend continued by the 7th day, with undrained samples showing a 36.7 % improvement compared to 26.6 % in drained samples.

The findings presented above indicate that higher magnitudes and rates of rockwall closure (within non-excessive limits) significantly enhance the consolidation behavior of CPB, with the most pronounced effects observed in drained conditions, particularly during the early stages of curing. This enhanced consolidation leads to notably improved mechanical strength, which is crucial for the structural stability of CPB. Additionally, the results demonstrate that drainage consistently facilitates faster and more efficient strength development in CPB. As underground mining operations progress to greater depths – conditions often accompanied by elevated rockwall closure stresses – it becomes imperative to consider the effects of multiaxial stresses, including horizontal stress induced by rockwall closure, on CPB consolidation and strength development. Incorporating these factors is

essential for designing cost-effective and structurally sound CPB systems in deep mining environments.

3.3. Impact of consolidation behavior under multiaxial stress loading on the deformations and strains of MCS-CPB during curing

Fig. 11 illustrates the evolution of deformations and strains in CPB under different multiaxial stress conditions – MCS1 and MCS2 – in both drained and undrained conditions. The impact of these stress conditions on CPB deformation behavior during the curing process over the 28-d period was examined, focusing on how varying levels of horizontal rockwall closure, vertical stress, and drainage affected the material's compressive response. On the top axes of the figure, the horizontal stress and vertical stress were also displayed for better comprehending the effect of multiaxial stress.

3.3.1. Initial curing phase (Days 0–4)

In the first 4 d of curing, the vertical stress (σ_V) step increased from 0 kPa to 610.08 kPa while the horizontal stress (σ_H) increased from 0 kPa to 60 kPa. Under undrained conditions, MCS1-UD-CPB displayed a rapid escalation in vertical deformation, reaching 2.571 mm (equivalent to a vertical strain of 1.607 %), and a slight increase in horizontal deformation, reaching 0.319 mm (equivalent to a horizontal strain of 0.591 %). Concurrently, the volumetric deformation reached 12.905 cm^3 (or a volumetric strain of 2.776 %). Under drained conditions (i.e. higher consolidation), the vertical deformation of MCS1-D-CPB increased more significantly, reaching 3.192 mm (equivalent to a vertical strain of 1.995 %) on the 4th day. The horizontal deformation also increased, reaching 0.467 mm (equivalent to a horizontal strain of 0.865 %). Both of them contributed to the volumetric deformation of 17.182 cm^3 (or a volumetric strain of 3.683 %).

During the initial phase of curing, CPB under both undrained and drained conditions experienced rapid initial deformations, particularly vertical deformation, due to the imposition of vertical stress from backfilling. This initial vertical deformation was accentuated in the drained condition because the expulsion of pore water allowed for greater particle rearrangement, leading to increased consolidation and settlement. The drained CPB

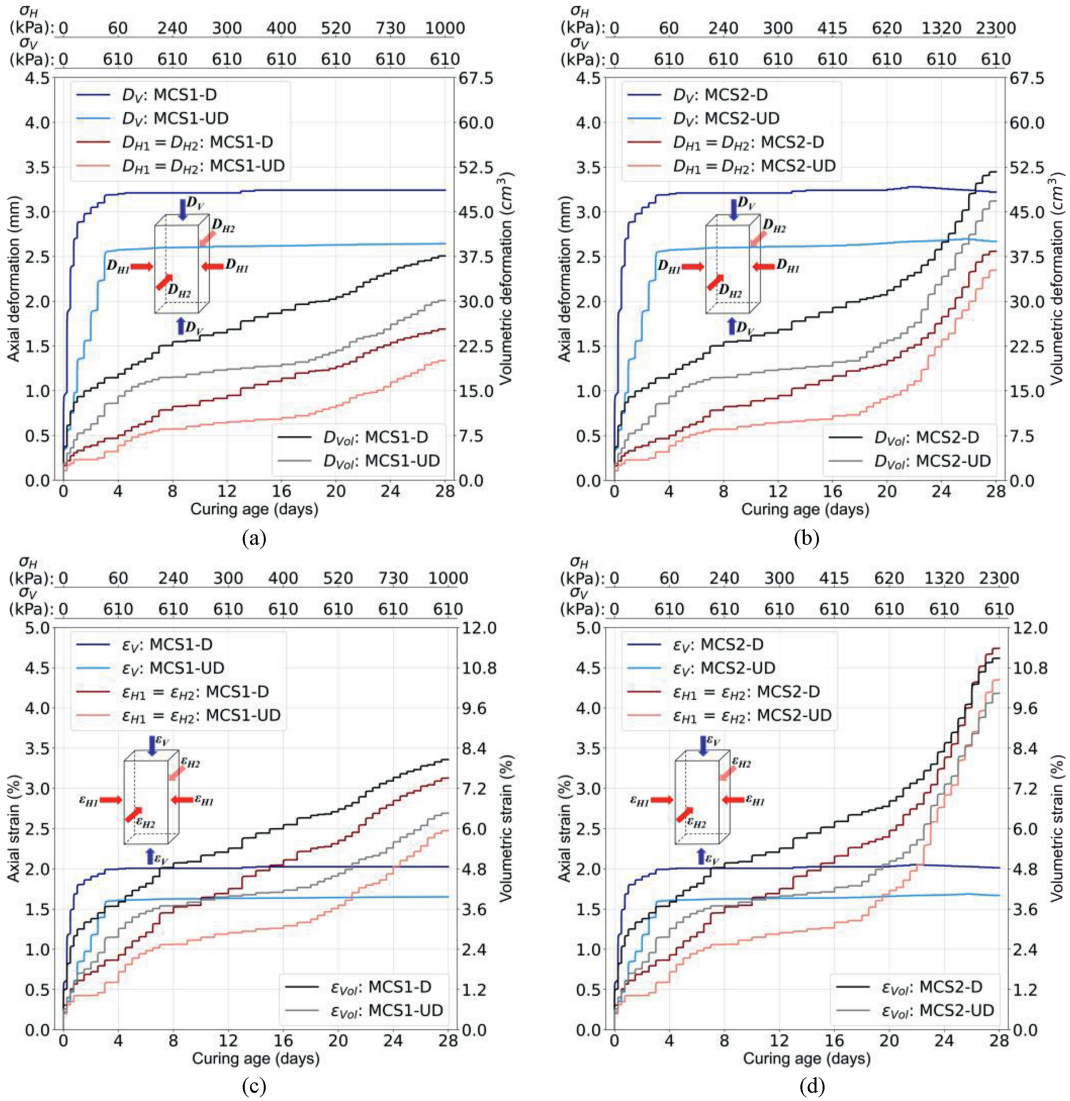

Fig. 11. Monitored deformation and strain of CPB under multiaxial stress conditions for both undrained and drained samples: (a) Deformation - MCS1, (b) Deformation - MCS2, (c) Strain - MCS1, and (d) Strain - MCS2 (D_V: vertical deformation; D_{H1}, D_{H2}: horizontal deformation; D_{vol}: volumetric deformation; ε_V: vertical strain; ε_{H1}, ε_{H2}: horizontal strain; ε_{vol}: volumetric strain).

demonstrated more significant vertical deformation as water was efficiently expelled through drainage, reducing pore pressure and increasing effective stress, which amplified vertical strain. In contrast, the undrained CPB exhibited less vertical deformation because the excess pore water could not escape through drainage, maintaining higher pore pressures that counteracted the applied stresses and limited deformation. The presence of pore water in the undrained condition provided temporary support against compression, resulting in lower initial deformations compared to the drained condition.

3.3.2. Intermediate curing phase (Days 4–14)

During this period, the vertical stress remained constant at 610.08 kPa (since backfilling was completed), while the horizontal stress continued to increase progressively. The horizontal stress increased from 60 kPa on the 4th day to 360 kPa on the 14th day.

After backfilling, the vertical deformation stabilized for both undrained and drained samples under multiaxial stress conditions. The vertical deformation of undrained samples (MCS1-UD-CPB) exhibited a slight rise from 2.571 mm on the 4th day to 2.614 mm on the 14th day (corresponding to a vertical strain increase from 1.607 % to 1.634 %). Similarly, the vertical deformation of drained samples (MCS1-D-CPB), which were subjected to higher consolidation, increased marginally from 3.192 mm on the 4th day to 3.231 mm on the 14th day (with a vertical strain increase from 1.995 % to 2.019 %). Therefore, the MCS1-UD-CPB increased more in terms of vertical deformation and strain over that period. In drained conditions, the pore water was allowed to escape, and much of the consolidation and associated deformation occurred earlier during the initial phase (0–4 d). After this initial consolidation, the rate of deformation reduced, resulting in a smaller increase between the 4th day and the 14th day. The minimal increase in vertical deformation during this phase was attributed to the cessation of vertical stress application and the ongoing cement hydration process, which increased the stiffness of the CPB (Fahey et al., 2011; Yilmaz et al., 2014; Zhao et al., 2021; Chen et al., 2022). In the drained condition, most consolidation due to vertical stress occurred during the initial phase, resulting in limited additional vertical deformation.

In addition, the horizontal deformation of MCS1-UD-CPB increased steadily from 0.319 mm on the 4th day to 0.661 mm on the 14th day (corresponding to a horizontal strain increase from 0.591 % to 1.224 %). The horizontal deformation of MCS1-D-CPB increased from 0.457 mm to 1.031 mm (with a horizontal strain from 0.865 % to 1.909 %) over the same period (Fig. 11).

The drained samples (MCS1-D-CPB) exhibited a greater increase in horizontal deformation between the 4th day and the 14th day compared to the undrained samples (MCS1-UD-CPB). The larger increase in horizontal deformation in the drained condition can be attributed to the effect of drainage on consolidation behavior. In the drained condition, excess pore water pressure generated by the applied horizontal stress was allowed to dissipate as water drained out of the CPB material. This reduction in pore water pressure increased the effective stress acting on the soil skeleton, leading to greater deformation. With the dissipation of pore water, the particles within the CPB rearranged under the increased effective stress (Helinski et al., 2006; Veenstra et al., 2015; Al-Moselly and Fall, 2024b). This rearrangement resulted in additional horizontal deformation as the material consolidated. The drainage facilitated consolidation settlement, allowing the CPB to deform more under the same applied stress compared to the undrained condition. In the undrained condition, the pore water pressure remained elevated, providing temporary resistance to deformation. Over time, as the CPB cured and gained strength due to cement hydration, the rate of deformation decreased. However, during the intermediate curing phase (Days 4–14), the effects of drainage were more pronounced, leading to greater increases in deformation in the drained samples.

Drained samples exhibited higher volumetric deformations due to reduced pore pressures, allowing particles to move more freely under horizontal stress (Fig. 11). The increased effective stress in drained conditions led to higher deformations compared to undrained conditions, where pore water restricted particle movement. The volumetric deformation of MCS1-UD-CPB increased from 12,905 mm^3 on the 4th day to 18,789 mm^3 on the 14th day (volumetric strain from 2.776 % to 4.027 %). The volumetric deformation of MCS1-D-CPB increased from 17,182 mm^3 on the 4th day to 26,711 mm^3 on the 14th day (volumetric strain from 3.683 % to 5.725 %). The cumulative effects of drainage were evident, with drained samples exhibiting higher volumetric deformations and strains. Drainage accelerated consolidation by allowing pore water to escape, increasing effective stress and leading to greater total deformation.

3.3.3. Late curing phase (Days 14–28)

During the late curing period (Days 14–28), while the vertical stress remained constant at 610.08 kPa (constant CPB structure height) for both MCS1 and MCS2 conditions, the horizontal stress continued to increase due to rockwall closure. In the MCS1 condition, the horizontal stress increased from 360 kPa on the 14th day to 1000 kPa on the 28th day. In contrast, the MCS2 condition experienced a more rapid escalation, with horizontal stress increasing from 360 kPa to 2300 kPa over the same period, reflecting a faster rockwall closure rate.

As shown in Fig. 11, in the MCS1-UD-CPB (undrained condition), the vertical strain showed a minimal increase from 1.634 % (vertical deformation of 2.614 mm) on the 14th day of curing to 1.651 % (vertical deformation of 2.642 mm) on the 28th day. This slight change suggested that the CPB had developed sufficient stiffness due to cement hydration, limiting further vertical deformation despite the increasing horizontal stress. The horizontal strain in MCS1-UD-CPB increased noticeably from 1.224 % to 2.474 % over the same period. This significant rise in horizontal strain contributed to the volumetric strain increasing from 4.027 % to 6.457 % between the 14th and 28th days of curing, highlighting the influence of the applied horizontal rockwall closure stress on overall deformation.

Comparatively, the MCS1-D-CPB (drained condition) exhibited a relatively stable vertical strain, with only a 0.007 % increase from 2.019 % on the 14th day to 2.026 % on the 28th day, which was even less than the undrained sample's increase of 0.017 %. This stability suggested that drainage facilitated the dissipation of pore water pressure, enhancing the CPB's resistance to vertical deformation. However, the horizontal strain in MCS1-D-CPB increased more substantially, from 1.909 % to 3.128 % during the same period. The greater horizontal strain in the drained samples led to the volumetric strain rising from 5.725 % to 8.059 %, indicating that drainage (higher consolidation), while reducing vertical deformation, allowed for increased horizontal deformation due to reduced pore pressure.

Turning to the MCS2 condition, the effects of faster rockwall closure and higher horizontal stress were more pronounced. In the MCS2-UD-CPB (undrained condition), the vertical strain increased slightly from 1.634 % on the 14th day to 1.686 % on the 26th day, when the horizontal stress reached 1860 kPa. Subsequently, the vertical strain decreased marginally to 1.669 % on the 28th day, indicating a subtle transition from vertical compression to extension, as the horizontal stress was much higher than the vertical stress applied to CPB. The horizontal strain in MCS2-UD-CPB increased significantly from 1.224 % on the 14th day to 4.350 % on

the 28th day, a more substantial rise compared to MCS1-UD-CPB (from 1.224 % to 2.472 %). This dramatic increase reflected the substantial impact of the rapidly increasing horizontal stress in MCS2. Consequently, the volumetric strain in MCS2-UD-CPB reached 10.038 % on the 28th day, emphasizing the significant deformation experienced under these conditions.

Similarly, in the MCS2-D-CPB (drained condition), the vertical strain increased from 2.019 % on the 14th day to 2.045 % on the 23rd day, when the horizontal stress was 1090 kPa. Afterward, the vertical strain decreased to 2.013 % on the 28th day of curing, indicating that the vertical extension commenced earlier in the drained sample compared to the undrained one. This earlier onset can be attributed to the horizontal strain in MCS2-D-CPB, which rose from 1.909 % on the 14th day to 4.741 % on the 28th day – exceeding the horizontal strain observed in MCS2-UD-CPB. The volumetric strain reached 11.084 % on the 28th day, indicating enhanced consolidation effects due to drainage under high horizontal stress.

The deformation behavior of CPB during curing was shown to be significantly impacted by the increase rate of horizontal stress during the period of Days 14–28. MCS2 samples exhibited greater deformations than MCS1 samples due to the increased magnitude of horizontal stresses from faster rockwall closure. Drained samples showed higher horizontal strains than undrained samples in both MCS1 and MCS2 conditions, indicating that drainage facilitated greater deformation or consolidation by allowing pore water to escape, reducing pore pressures, and increasing effective stress. This effect was more pronounced in the MCS2 condition due to the faster rate of rockwall closure and higher horizontal stresses, emphasizing the significant role of drainage in the consolidation behavior of CPB under multiaxial stress conditions. These findings highlighted the necessity of considering both drainage conditions and the rate of rockwall closure in the design and management of CPB structures to ensure structural integrity and stability during curing under multiaxial stress conditions.

3.4. Impact of consolidation behavior under multiaxial stress loading on the stress-strain curves of CPB

Fig. 12 compares the stress-strain behaviour of CPB subjected to stress-free and multiaxial stress conditions for both undrained and drained samples at different curing ages. The typical stress-strain curve for CPB, a cement-based material, consists of an initial elastic (linear) phase, followed by a nonlinear phase where microcracks develop, leading to peak stress (UCS), and then a post-peak phase that may include strain softening or brittle failure. According to previous research (Chen et al., 2021), the stress-strain curve of CPB can be divided into four phases: initial compaction, linear elastic phase, nonlinear plastic phase, and post-peak damage phase. The peak strain and peak stress occur between the nonlinear plastic phase and post-peak damage phase, a phenomenon referred to as peak behavior, which will be discussed further. Each phase offers valuable insights into the response of material to load.

3.4.1. Initial compaction phase

As shown in Fig. 12a, the initial compaction phase (pre-linear elastic phase) occurred at very low strain levels, near the beginning of the stress-strain curve and ended quickly. During this phase, slight compression of the CPB material occurred as voids were compacted before the CPB material entered its linear elastic response. This behavior is typical of cement-based materials like CPB, where the initial voids are reduced before elastic deformation begins. In Fig. 12a, this phase is marked by a subtle curvature at the start of each curve, where the slope is initially low before it steepens.

This compaction phase was more pronounced at early curing stages, such as at 1 and 3 d, particularly in undrained samples, where excessive pore water pressure hinders initial consolidation. Multiaxial stress conditions also influenced this behavior. Both drained (MCS1-D-CPB) and undrained (MCS1-UD-CPB) samples under multiaxial stress exhibited a less pronounced compaction phase compared to control samples on the first day of curing, suggesting that the applied multiaxial stress induced a more compact structure early in the curing process. As curing progressed, the duration of this compaction phase shortened further, as seen in the reduced compaction in CPBs at 3 d of curing (Fig. 12b). By the 7th day of curing (Fig. 12c), the compaction phase became less significant across all samples, and by 28th day, it was almost completely diminished (Fig. 12d and e). This is because the hydration process strengthened the CPB matrix, leading to a stronger pore structure with fewer initial voids.

3.4.2. Linear elastic phase

Following the initial compaction, the CPB exhibited linear elastic behavior, where stress increased linearly with strain. This phase represents the ability of CPB material to elastically deform without permanent damage, meaning it can return to its original shape if the load is removed. In Fig. 12a, this linear phase is visible in the steep portion of each curve following the compaction phase. For instance, on the first day of curing age, drained samples showed a steeper slope during the linear elastic phase, indicating greater stiffness. This increased stiffness in drained samples, particularly under multiaxial stress (MCS1-D-CPB), reflected greater consolidation, where the solid matrix carried more of the applied load due to the removal of pore water. In contrast, in undrained samples, such as MCS1-UD-CPB and Control-UD-CPB, the linear elastic phase was less steep, indicating lower stiffness due to the retained pore water, which reduced effective stress and impeded the load-bearing capacity. As the curing progressed to 3, 7, and 28 d (Fig. 12b–e), the slope of the linear elastic phase steepened across all CPB samples, reflecting the increasing stiffness of CPB due to ongoing hydration and consolidation. Drained samples, especially under multiaxial stress, consistently exhibited the steepest slopes, demonstrating the beneficial effect of drainage or higher consolidation in enhancing the stiffness and load-bearing capacity of CPB over time. Additionally, the steepness of the linear elastic phase directly relates to the elastic modulus of the CPB, which will be discussed in further detail in Section 3.2.4.

3.4.3. Nonlinear plastic phase

As the material was loaded further, it transitioned from elastic to nonlinear plastic behavior, where microcracks started to develop, leading to irreversible deformation. The nonlinear phase is observed where the curves begin to bend after the linear elastic phase (Fig. 12a), signalling that the CPB material was no longer deforming elastically and was accumulating permanent deformation. In this phase, both multiaxial stress and drainage conditions played crucial roles. Samples cured under multiaxial stress, whether drained or undrained, showed the onset of the nonlinear plastic phase at higher stress levels and lower strains compared to control (stress-free) conditions. This indicated that multiaxial stress during the curing process enhanced the CPB material's ability to withstand greater loads before yielding. Additionally, the nonlinear plastic phase is notably shorter in drained samples (MCS1-D-CPB and Control-D-CPB) (subjected to higher consolidation), which consistently reach higher stress levels and undergo lower strains compared to undrained samples (MCS1-UD-CPB and Control-UD-CPB). This suggests that drainage improves the resistance of CPB to plastic deformation by facilitating better consolidation and load-bearing capacity.

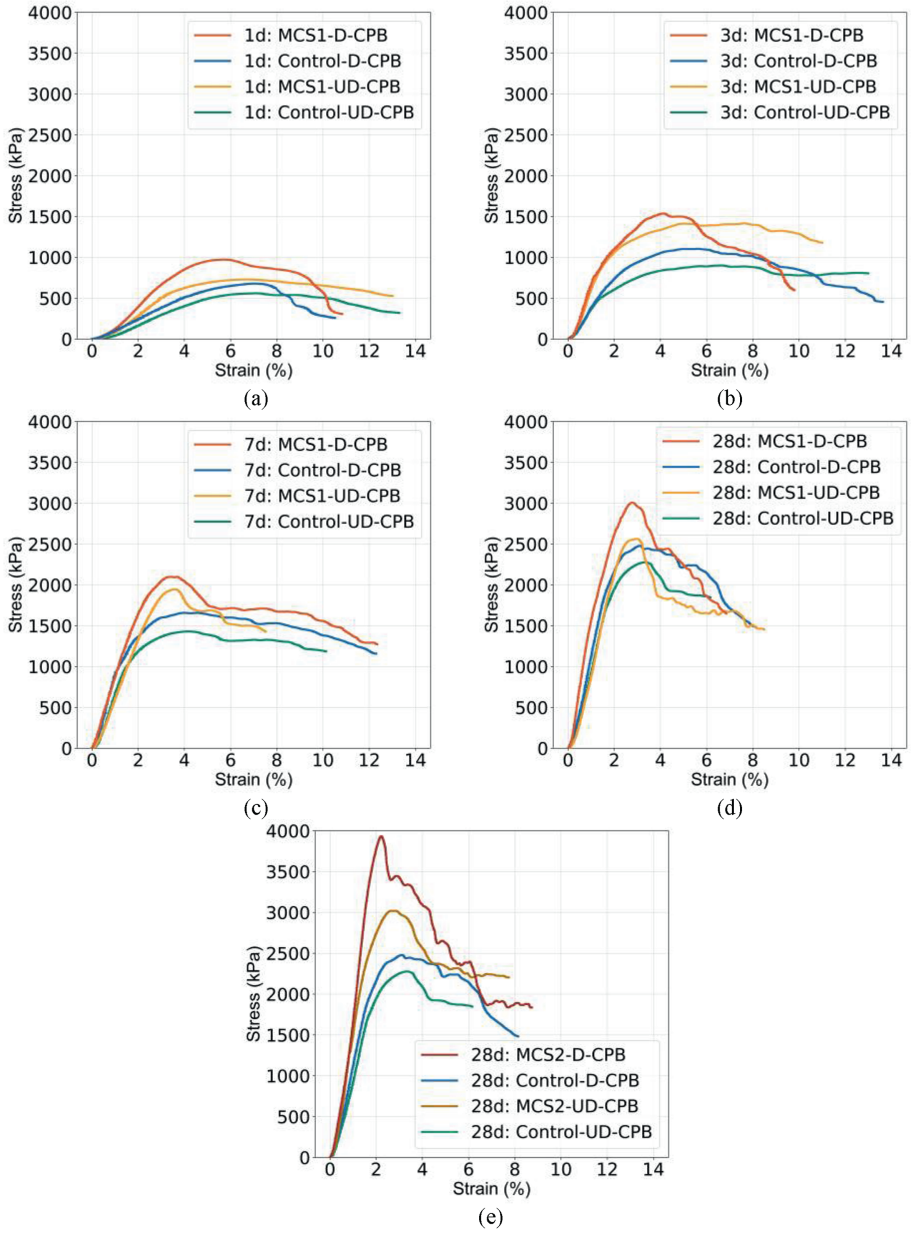

Fig. 12. Stress-strain comparison of CPB under stress-free and multiaxial stress conditions for both undrained and drained samples at different curing ages: (a) 1 d - MCS1, (b) 3 d - MCS1, (c) 7 d- MCS1, (d) 28 d - MCS1, and (e) 28 d - MCS2.

As shown in Fig. 12, the length of the nonlinear plastic phase progressively shortened as curing advanced. On the first day of curing, both drained and undrained control samples exhibited relatively long nonlinear plastic phases, indicating that more plastic deformation occurred before the CPB material reached peak stress, typical of early-stage curing. By the third day of curing, however, the nonlinear plastic phase became shorter in both drained and undrained samples, suggesting that as hydration progressed, the material consolidated, and the extent of plastic deformation reduced. This trend continued over time, reflecting improved resistance to plastic deformation and increased peak strength. The influence of multiaxial stress further shortened nonlinear plastic phases, particularly in drained samples, i.e. in samples with higher degree of consolidation. For both the first and third days of curing age, the samples subjected to multiaxial stress (especially MCS1-D-CPB) exhibited consistently shorter nonlinear plastic phases compared to control samples, reflecting the compounding effect of multiaxial stress and drainage or consolidation on limiting plastic deformation.

3.4.4. Peak behavior

The transition between the nonlinear plastic phase and the post-peak damage phase is marked by the material reaching its peak stress and strain. The behavior at this point provides critical insight into the material's maximum load-bearing capacity and the maximum deformation before failure occurs.

Across all curing ages (1, 3, 7, and 28 d), drained samples exhibited higher peak stress and lower peak strain compared to undrained samples. For example, after 3 d of curing, the peak stress for MCS1-D-CPB (1.536 MPa) was higher than for MCS1-UD-CPB (1.412 MPa), while the peak strain for the drained sample (4.18 %) was lower than for the undrained sample (5.05 %). This behavior

was attributed to the efficient consolidation of drained samples, where the removal of excess pore water led to denser particle packing and a stiffer material with a higher load-bearing capacity.

Additionally, samples under multiaxial stress conditions exhibited increased peak stress and reduced peak strain compared to the control samples under stress-free conditions. For instance, after 7 d of curing, MCS1-D-CPB exhibited a peak stress of 2.098 MPa compared to that (1.657 MPa) of Control-D-CPB, with a lower peak strain (3.43 % vs. 3.99 %). The application of multiaxial stress enhanced the material's resistance to deformation and increased its load-bearing capacity, which resulted in higher peak stresses and lower peak strains.

As curing progressed, all samples, whether drained or undrained, stress-free or multiaxial, showed a consistent decrease in peak strain while peak stress increased. This was due to ongoing hydration, consolidation, and strengthening of the CPB, which resulted in a less deformable material over time. These trends in peak stress and strain behavior are crucial in understanding the transition from the nonlinear plastic phase to the post-peak damage phase, as they reveal the material's maximum strength and how it deforms under load before failure.

3.4.5. Post-peak damage phase

Post-peak damage behavior represents the response of CPB material after reaching peak stress, where it either undergoes brittle failure or strain softening. In Fig. 12, this phase is characterized by the decline in stress after the peak. The behavior in this phase was heavily influenced by both drainage and curing stress conditions.

Drained samples, especially those under multiaxial stress (MCS1-D-CPB), exhibited a faster post-peak drop, indicating a more brittle failure. This was due to the better-consolidated structure formed in drained samples during curing, which quickly lost its load-bearing capacity after reaching peak stress. For example, after 3 d of curing (Fig. 12b), MCS1-D-CPB exhibited a more pronounced post-peak decline compared to MCS1-UD-CPB, which showed a more gradual decrease in stress, reflecting strain softening. This soft-straining behavior was typical of undrained samples, where the presence of more pore water delayed the collapse of the internal structure, leading to a ductile failure mechanism. As curing progresses, the difference in post-peak behavior caused by drainage conditions becomes less severe. As seen in Fig. 12c–e, the drained samples showed a stress drop similar to that of undrained samples for both multiaxial stress conditions and stress-free conditions. However, drained samples still demonstrated a steeper post-peak decline, reflecting their more consolidated structure and higher peak strength. This suggests that their ability to withstand stress is enhanced due to effective drainage during curing.

In addition to the influence of drainage, the multiaxial stress conditions also significantly affected post-peak behavior. Under drained conditions, multiaxial stress accelerated the expulsion of the pore water, especially during the early curing ages (Days 0–7). This resulted in a more brittle failure of the MCS1-D-CPB samples compared to the Control-D-CPB samples. By the 28th day of curing, this difference in behavior between these samples became less. However, as shown in Fig. 12e, the MCS2-D-CPB, cured under faster rockwall closure conditions, exhibited a greater brittle failure than MCS1-D-CPB. This expanded the difference compared to the Control-UD-CPB samples, indicating that faster multiaxial compression further enhanced the pore structure. Conversely, the multiaxial stress compressed the CPB under undrained conditions, but pore water cannot escape. As a result, MCS1-UD-CPB samples showed a gradual stress drop post-peak, similar to the Control-UD-CPB samples on the first and third days of curing. After 7 d of curing, the MCS1-UD-CPB samples consumed water more quickly, leading to increased brittleness and a faster stress drop after the peak compared to the Control-UD-CPB. By the 28th day of curing, the Control-UD-CPB samples also began to show brittle failure, but they remained less brittle than the MCS1-UD-CPB due to the effects of the multiaxial stress.

Overall, the failure mode of CPB was strongly influenced by the curing stress conditions, although all specimens were tested under unconfined compression. CPB cured under stress-free conditions generally exhibited strain-softening behavior, particularly at early curing ages, indicative of a more ductile failure mode. When cured under multiaxial stress loading (MCS1), the CPB samples became progressively more brittle, especially under drained conditions, due to enhanced consolidation and reduced pore space. Notably, CPB samples cured under faster rockwall closure conditions (MCS2) exhibited a significantly sharper post-peak stress drop during UCS testing, indicating a clear shift toward a brittle failure mode. This was particularly evident in drained MCS2-CPB samples, where the post-peak decline was more abrupt compared to MCS1-CPB samples. These results show that higher curing confinement (even if removed during unconfined compression testing) promotes microstructural densification, reduces ductility, and alters the post-peak failure behavior of CPB toward more brittle fracture mechanisms.

3.5. Impact of consolidation behavior under multiaxial stress loading on the modulus of elasticity development of CPB

Fig. 13 presents the development of the modulus of elasticity for CPB samples across different curing ages and conditions. These data reflect how multiaxial stress and drainage conditions affect the stiffness and elastic behavior of CPB over time. In this study, the reported elastic modulus corresponds to the tangent modulus (E_t), defined as the slope of the stress–strain curve at the point corresponding to 50 % of the peak stress. This calculation method was adopted because the stress–strain behavior of CPB is nonlinear, and using the modulus at 50 % of the peak stress ensures that the measured stiffness represents the primarily elastic phase of deformation, before the onset of significant plasticity or microcrack propagation. Selecting a consistent reference point within the elastic range enables reliable comparisons between CPB specimens cured under different multiaxial stress and drainage conditions.

As curing progressed, the tangent modulus of CPB increased across all conditions, although the rate of growth slowed over time. Between the first and third days of curing, there was a significant rise in modulus for both undrained and drained samples, with MCS1-UD-CPB and MCS1-D-CPB showing a considerable improvement of over 150 %. After the 7th day of curing, the rate of increase slowed considerably. For example, the modulus of MCS1-UD-CPB increased by less than 110 % over the longer period from the 7th day to the 28th day, with drained samples following a similar trend. This deceleration in modulus growth is typical as hydration slows and the material structure stabilizes.

This pattern of modulus increase over time is further influenced by multiaxial stress, which significantly enhances the modulus of elasticity, especially under drained conditions. This effect is evident in the consistent outperformance of CPB under multiaxial stress compared to control samples. For example, on Day 1, the tangent modulus of MCS1-UD-CPB reached 23.0 MPa, nearly double that of the Control-UD-CPB (11.7 MPa), showing a 96.6 % increase. A similar trend was seen in the drained condition, where MCS1-D-CPB achieved 28.7 MPa compared to 13.8 MPa for Control-D-CPB, reflecting a 107.6 % increase. These early-stage increases highlight the beneficial impact of multiaxial stress on

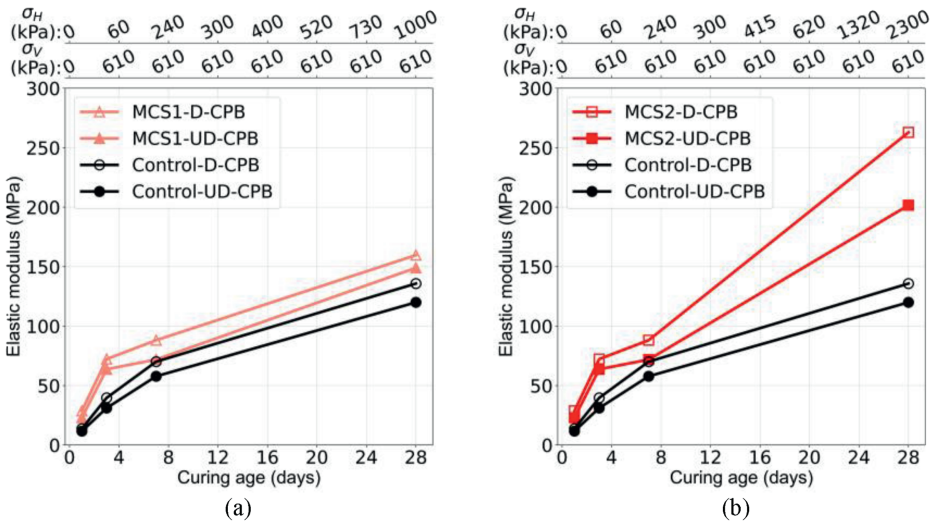

Fig. 13. Elastic modulus development of CPB cured under multiaxial stress loadings for undrained and drained conditions: (a) MCS1-CPB, and (b) MCS2-CPB.

modulus development, likely due to the enhanced particle compaction and accelerated hydration reactions facilitated by the applied multiaxial stresses.

In the later curing stages, however, the effect of multiaxial stress under MCS1 conditions began to reduce. Between the 14th and 28th d of curing, where the horizontal stress increased from 360 kPa to 1000 kPa, the tangent modulus of MCS1-UD-CPB reached 148.9 MPa by day 28, only 24.2 % higher than the 119.9 MPa observed in Control-UD-CPB. Similarly, in drained samples, MCS1-D-CPB reached 159.6 MPa, which was 17.6 % higher than the 135.8 MPa in Control-D-CPB.

In contrast, under MCS2 conditions, where the horizontal stress increased noticeably from 360 kPa to 2300 kPa, the modulus of elasticity showed much larger gains by day 28. The tangent modulus of MCS2-UD-CPB reached 201.6 MPa, a significant 68 % higher than the Control-UD-CPB value of 119.9 MPa. In drained samples, the difference was even more pronounced, with MCS2-D-CPB reaching 262.8 MPa, a substantial 93.5 % higher than the 135.8 MPa observed in Control-D-CPB. This comparison highlights the more intense impact of the higher rockwall closure-induced horizontal stress in MCS2 conditions, leading to greater increases in modulus, particularly in drained samples.

In addition to multiaxial stress, drainage also plays a crucial role in improving the modulus of elasticity. For instance, at 1 day of curing, the tangent modulus (13.8 MPa) of Control-D-CPB was 17.9 % higher than that (11.7 MPa) of Control-UD-CPB. The same pattern was seen under multiaxial stress, where the tangent modulus (28.7 MPa) of MCS1-D-CPB on the first day of curing was 24.8 % higher than that (23.0 MPa) of MCS1-UD-CPB.

Ultimately, these data indicate that faster and higher multiaxial stresses, as seen in MCS2, further accelerate the modulus development, especially in the later curing stages. The substantial increase in modulus under MCS2 conditions can be attributed to more efficient particle compaction and accelerated hydration caused by the higher stress levels, particularly in drained conditions where water expulsion further promotes the stiffening of the material.

4. Conclusions

This study employed a novel multiaxial stress curing and monitoring apparatus to simulate two rockwall closure scenarios, examining both drained and undrained conditions to assess the consolidation behavior of CPB and its impact on key material mechanical properties. The findings demonstrate that multiaxial stress, horizontal stress-induced by rockwall closure, and drainage conditions significantly influence consolidation behavior and, in turn, affect the development of CPB's mechanical properties (strength, deformation, stress-strain behaviour, elastic of modulus).

Multiaxial stress played critical roles in accelerating consolidation. Higher horizontal stress, particularly under faster rockwall closure, enhances particle rearrangement, reduces void ratios, and accelerates consolidation, especially during later curing stages. Effective drainage further accelerates consolidation by facilitating pore water expulsion, leading to lower void ratios and more efficient particle packing. Multiaxial stress also interacts with drainage conditions, with elevated horizontal stresses reducing the differences in consolidation behavior between drained and undrained samples at higher stress levels.

The consolidation behavior impacted the development of key CPB mechanical properties such as UCS, deformation, stress-strain behavior, and modulus of elasticity. Higher and faster rockwall closure/multiaxial stress and effective drainage promoted greater consolidation, leading to increased UCS, more rapid deformation and strain evolution during curing, and improved stiffness, as reflected in steeper stress-strain curves. These conditions also contributed to a higher modulus of elasticity, indicating enhanced material rigidity and load-bearing capacity. Furthermore, the study highlighted that the drained conditions facilitated the earlier onset of the nonlinear plastic phase and higher peak stresses, while the combined effects of multiaxial stress and drainage led to more brittle failure in the post-peak phase.

In conclusion, this research demonstrates the importance of considering multiaxial stress, rockwall closure and drainage conditions in the design and implementation of CPB structures, as these factors significantly influence consolidation behavior and the development of mechanical properties essential for ensuring stability and performance throughout the whole curing process.

While this study provides significant insights into the consolidation behavior of CPB under varying multiaxial stress and drainage conditions, other influential factors remain underexplored. In particular, PSD, tailings gradation, and microstructural changes on consolidation dynamics has not been thoroughly

examined, even though these factors play a vital role in the evolution of porosity and the development of mechanical properties. Given the substantial variability of tailings characteristics across different mining operations, future studies are encouraged to investigate how different PSD profiles and gradation curves affect the consolidation behavior and mechanical response of CPB under multiaxial stress curing conditions. Such research would provide important guidance for optimizing backfill design tailored to specific site conditions. In addition, advanced microstructural characterization techniques, such as scanning electron microscopy (SEM) and X-ray computed tomography (XCT), could be employed to directly link microstructural changes to macroscopic mechanical performance. Expanding research efforts in these areas will contribute to a more comprehensive understanding of CPB behavior and further support the development of more reliable and efficient backfilling strategies in underground mining environments, particularly those involving progressive rockwall closure.

CRediT authorship contribution statement

Hongbin Liu: Writing – original draft, Visualization, Software, Methodology, Investigation, Conceptualization. **Mamadou Fall:** Writing – review & editing, Supervision, Resources, Project administration, Methodology, Funding acquisition, Conceptualization.

Declaration of competing interest

The authors declare that they have no known competing financial interests or personal relationships that could have appeared to influence the work reported in this paper.

Acknowledgments

The first author would like to thank the University of Ottawa, Natural Sciences and Engineering Research Council of Canada (NSERC) and the China Scholarship Council for their financial support.

References

Aldhafeeri, Z., Fall, M., 2017. Sulphate induced changes in the reactivity of cemented tailings backfill. Int. J. Miner. Process. 166, 13–23.
Al-Moselly, Z., Fall, M., 2024a. Investigating pore water pressure development in paste backfill under conditions mimicking field loading. Geotech. Geol. Eng. 42, 3491–3514.
Al-Moselly, Z., Fall, M., 2024b. Multiphysical testing of strength development of cemented paste backfill containing superplasticizer. Cement Concr. Compos. 154, 105772.
Al-Moselly, Z., Fall, M., 2022. Further insight into the strength development of cemented paste backfill containing polycarboxylate ether-based superplasticizer. J. Build. Eng. 47, 103859.
Belem, T., El Aatar, O., Bussière, B., Benzaazoua, M., 2016. Gravity-driven 1-D consolidation of cemented paste backfill in 3-m-high columns. Innov. Infrastruct. Solut. 1 (1), 37.
Benzaazoua, M., Belem, T., Bussière, B., 2002. Chemical factors that influence the performance of mine sulphidic paste backfill. Cement Concr. Res. 32 (7), 1133–1144.
Chen, S., Wu, A., Wang, Y., Wang, W., 2021. Coupled effects of curing stress and curing temperature on mechanical and physical properties of cemented paste backfill. Constr. Build. Mater. 273, 121746.
Chen, S., Xiang, Z., Eker, H., 2022. Curing stress influences the mechanical characteristics of cemented paste backfill and its damage constitutive model. Buildings 12 (10), 1607.
Cheng, H., Wu, S., Li, H., Zhang, X., 2020. Influence of time and temperature on rheology and flow performance of cemented paste backfill. Constr. Build. Mater. 231, 117117.
Cui, L., Fall, M., 2016. Mechanical and thermal properties of cemented tailings materials at early ages: influence of initial temperature, curing stress and drainage conditions. Constr. Build. Mater. 125, 553–563.
Cui, L., Fall, M., 2017a. Multiphysics model for consolidation behavior of cemented paste backfill. Int. J. GeoMech. 17 (3), 04016077.
Cui, L., Fall, M., 2017b. Modeling of pressure on retaining structures for underground fill mass. Tunnel. Underg. Sp. Tech 69, 94–107.
Cui, L., Fall, M., 2018. Multiphysics modeling and simulation of strength development and distribution in cemented tailings backfill structures. Int. J. Concr. Struct. Mat. 12, 1–22.
Doherty, J.P., 2015. A numerical study into factors affecting stress and pore pressure in free draining mine stopes. Comput. Geotech. 63, 331–341.
Fahey, M., Helinski, M., Fourie, A., 2010. Consolidation in accreting sediments: Gibson's solution applied to backfilling of mine stopes. Geotechnique 60 (11), 877–882.
Fahey, M., Helinski, M., Fourie, A., 2011. Development of specimen curing procedures that account for the influence of effective stress during curing on the strength of cemented mine backfill. Geotech. Geol. Eng. 29 (5), 709–723.
Fall, M., Benzaazoua, M., Saa, E.G., 2008. Mix proportioning of underground cemented tailings backfill. Tunn. Undergr. Space Technol. 23 (1), 80–90.
Fall, M., Samb, S.S., 2009. Effect of high temperature on strength and microstructural properties of cemented paste backfill. Fire Saf. J. 44 (4), 642–651.
Fall, M., Wu, D., Pokharel, M., 2014. Effect of deep mine temperature conditions on the heat development in cemented paste backfill and its properties. In: Hudyma, M., Potvin, Y. (Eds.), Deep Mining 2014 - Proceedings of the Seventh International Conference on Deep and High Stress Mining. Australian Centre for Geomechanics, Perth, pp. 559–573.
Fang, K., Fall, M., 2018. Effects of curing temperature on shear behaviour of cemented paste backfill-rock interface. Int. J. Rock Mech. Min. Sci. 112, 184–192.
Fang, K., Fall, M., 2019. Chemically induced changes in the shear behaviour of interface between rock and tailings backfill undergoing cementation. Rock Mech. Rock Eng. 52 (9), 3047–3062.
Fang, K., Fall, M., 2020. Insight into the mode I and mode II fracture toughness of the cemented backfill-rock interface: effect of time, temperature and sulphate. Constr. Build. Mater. 262, 120860.
Geng, W., Wang, W., Huang, G., Jiang, C., Song, Z., Guo, S., Dong, Z., 2024. Case study on the secondary support time and optimization of combined support for a roadway under high in-situ stress. Geomech. Geophys. Geo-Energy Geo-Resour. 10 (1), 66.
Ghirian, A., Fall, M., 2015. Coupled behavior of cemented paste backfill at early ages. Geotech. Geol. Eng. 33, 1141–1166.
Ghirian, A., Fall, M., 2016. Strength evolution and deformation behaviour of cemented paste backfill at early ages: effect of curing stress, filling strategy and drainage. Int. J. Min. Sci. Technol. 26 (5), 809–817.
Grabinsky, M., Simms, P., Jewell, R., Lawson, S., Newman, P., 2006. Self-desiccation of cemented paste backfill and implications for mine design. In: Jewell, R., Lawson, S., Newman, P. (Eds.), Paste 2006 - Proceedings of the Ninth International Seminar on Paste and Thickened Tailings. Austr. Centre for Geomechanics, pp. 323–332.
Gric, A.G., 2001. Recent minefill developments in Australia. In: Proceedings of the 7th International Symposium on Mining with Backfill: Minefill, pp. 351–357.
Hasan, A., Suazo, G., Fourie, A.B., Jewell, R., Fourie, A.B., Caldwell, J., Pimenta, J., 2013. Full scale experiments on the effectiveness of a drainage system for cemented paste backfill. In: Jewell, R., Fourie, A.B., Caldwell, J., Pimenta, J. (Eds.), Paste 2013 - Proceedings of the 16th International Seminar on Paste and Thickened Tailings Australian Centre for Geomechanics, pp. 379–392.
Hassani, F., Fotoohi, K., Doucet, C., 1998. Instrumentation and backfill performance in a narrow vein gold mine. Int. J. Rock Mech. Min. Sci. 35 (4), 392.
He, Q., Cao, S., Yilmaz, E., 2025. Characterizing mechanical and multiscale porosity features of cementitious high sulfur tailings backfill using CT technology. Process Saf. Environ. Prot. 194, 858–872.
Helinski, M., Fourie, A.B., Fahey, M., 2006. Mechanics of early age cemented paste backfill. In: Jewell, R., Lawson, S., Newman, P. (Eds.), Paste 2006 - Proceedings of the Ninth International Seminar on Paste and Thickened Tailings. Australian Centre for Geomechanics, Perth, pp. 313–322.
Hou, C., Zhu, W., Yan, B., Guan, K., Du, J., 2018. Influence of binder content on temperature and internal strain evolution of early age cemented tailings backfill. Constr. Build. Mater. 189, 585–593.
Jafari, M., Shahsavari, M., Grabinsky, M., 2020. Cemented paste backfill 1-D consolidation results interpreted in the context of ground reaction curves. Rock Mech. Rock Eng. 53 (9), 4299–4308.
Jaouhar, E.M., Li, L., 2019. Effect of drainage and consolidation on the pore water pressures and total stresses within backfilled stopes and on barricades. Adv. Civ. Eng. 2019, 1–19.
Junior, A.N., Filho, R.D.T., Fairbairn, E. de M.R., Dweck, J., 2012. Early stages hydration of high initial strength Portland cement: part I. thermogravimetric analysis on calcined mass basis. J. Therm. Anal. Calorim. 108 (2), 725–731.
Kesimal, A., Yilmaz, E., Ercikdi, B., Alp, I., Deveci, H., 2005. Effect of properties of tailings and binder on the short-and long-term strength and stability of cemented paste backfill. Mater. Lett. 59 (28), 3703–3709.
Li, W., Fall, M., 2016. Sulphate effect on the early age strength and self-desiccation of cemented paste backfill. Constr. Build. Mater. 106, 296–304.
Liu, H., Fall, M., 2024. Testing the properties of cemented tailings backfill under multiaxial compressive loading. Constr. Build. Mater. 421, 135682.
Lu, G., Selvadurai, A.P.S., Meguid, M.A., 2024a. Analytical solution to non-isothermal pore-pressure evolution in hydrating minefill. Can. Geotech. J. 61 (12), 2722–2734.
Lu, G.D., Selvadurai, A.P.S., Meguid, M., 2024b. Aquathermal effect of anomalous pressure generation in consolidating minefill. Geotech 75 (5), 612–621.
Ma, Q., Liu, G., Yang, X., Guo, L., 2023. Physical model investigation on effects of

drainage condition and cement addition on consolidation behavior of tailings slurry within backfilled stopes. Int. J. Min. Metal. Mat. 30 (8), 1490–1501.
Maurya, T., Karena, K., Vardhan, H., Aruna, M., Raj, M.G., 2015. Potential sources of heat in underground mines – a review. Procedia Earth Planet. Sci. 11, 463–468.
Muir Wood, D., Doherty, J.P., 2014. Coupled chemical shrinkage and consolidation: some benchmark solutions. Transp. Por. Med. 105 (2), 349–370.
Naidu, G., Ryu, S., Thiruvenkatachari, R., Choi, Y., Jeong, S., Vigneswaran, S., 2019. A critical review on remediation, reuse, and resource recovery from acid mine drainage. Environ. Pollut. 247, 1110–1124.
Qin, J., Zheng, J., Li, L., 2021. Experimental study of the shrinkage behavior of cemented paste backfill. J. Rock Mech. Geotech. Eng. 13 (3), 545–554.
Raffaldi, M.J., Seymour, J.B., Richardson, J., Zahl, E., Board, M., 2019. Cemented paste backfill geomechanics at a narrow-vein underhand cut-and-fill mine. Rock Mech. Rock Eng. 52 (12), 4925–4940.
Rawlings, C., Phillips, H., 2001. Reduction of mine heat loads. In: Proceedings of the 7th International Mine Ventilation Congress, pp. 381–389.
Ruan, Z., Fu, H., Wu, A., Bürger, R., Wang, J., 2023. Utilization of rice straw as an inhibitor of strength deterioration of sulfide-rich cemented paste backfill. J. Mater. Res. Technol. 24, 833–843.
Ruan, Z., Wu, A., Bürger, R., Betancourt, F., Wang, Y., Wang, Y., Jiao, H., Wang, S., 2021. Effect of interparticle interactions on the yield stress of thickened flocculated copper mineral tailings slurry. Powder Technol. 392, 278–285.
Sari, M., Yilmaz, E., Kasap, T., Guner, N.U., 2022. Strength and microstructure evolution in cemented mine backfill with low and high pH pyritic tailings: effect of mineral admixtures. Constr. Build. Mater. 328, 127109.
Seymour, J.B., Raffaldi, M.J., Abraham, H., 2017. Monitoring the in situ performance of cemented paste backfill at the lucky Friday mine. In: Minefill 2017: Proceedings of the 12th International Symposium on Mining with Backfill, pp. 19–22.
Shahsavari, M., Grabinsky, M., 2014. Cemented paste backfill consolidation with deposition-dependent boundary conditions. In: Proceedings of the 67th Canadian Geotechnical Conference, vol. 28. Regina, Canada.
Sivakugan, N., 2008. Drainage issues and stress developments within hydraulic fill mine stopes. Aust. J. Civ. Eng. 5 (1), 61–70.
Song, X., Hao, Y., Huang, J., Wang, S., Liu, W., 2023. Study on mechanical properties and destabilization mechanism of unclassified tailings consolidation body under the action of dry-wet cycle. Constr. Build. Mater. 365, 130022.
Song, X., Hao, Y., Wang, S., Zhang, L., Liu, H., Yong, F., Dong, Z., Yuan, Q., 2022. Dynamic mechanical response and damage evolution of cemented tailings backfill with alkalized rice straw under SHPB cycle impact load. Constr. Build. Mater. 327, 127009.
Sun, W., Wang, H., Hou, K., 2018. Control of waste rock-tailings paste backfill for active mining subsidence areas. J. Clean. Prod. 171, 567–579.
Sun, W., Xue, Y., Li, T., Liu, W., 2019. Multi-field coupling of water inrush channel formation in a deep mine with a buried fault. Mine Water Environ. 38 (3), 528–535.
Sun, W., Zhang, S., Guo, W., Liu, W., 2017. Physical simulation of high-pressure water inrush through the floor of a deep mine. Mine Water Environ. 36 (4), 542–549.
Thompson, B.D., Grabinsky, M.W., Bawden, W.F., 2009. In-situ measurements of cemented paste backfill in long-hole stopes. In: ROCKENG09: Proceedings of the 3rd CANUS Rock Mechanics Symposium, Toronto, pp. 197–198.
Tian, X., Fall, M., 2021. Non-isothermal evolution of mechanical properties, pore structure and self-desiccation of cemented paste backfill. Constr. Build. Mater. 297, 123657.
Veenstra, R.L., Grice, A.G., Grabinsky, M.W., Bawden, W.F., Jewell, R., Fourie, A.B., 2015. Early curing age paste backfill exposures – the role of effective stress. In: Paste 2015: Proceedings of the 18th International Seminar on Paste and Thickened Tailings. Australian Centre for Geomechanics, pp. 329–340.
Wang, J., Wu, A., Wang, M., Ruan, Z., 2022a. Experimental investigation on flow behavior of paste slurry transported by gravity in vertical pipes. Processes 10 (9), 1696.
Wang, S., Wang, Z., Wu, A., Bi, C., Zhang, M., Liu, W., 2024. Bleeding, flowabilities, rheology, mechanical properties and strength deterioration mechanism of sulphide-rich cemented paste backfill. Constr. Build. Mater. 421, 135690.
Wang, Y., Fall, M., Wu, A., 2016. Initial temperature-dependence of strength development and self-desiccation in cemented paste backfill that contains sodium silicate. Cement Concr. Compos. 67, 101–110.
Wang, Y., Na, Q., Zhang, L., 2022b. Monitoring of in-situ properties for cemented tailings backfill that under drainage condition. Constr. Build. Mater. 356, 129254.
Wang, Z., Yang, C., Yang, P., Lyu, W., Yu, G., 2018. Study of the backfill confined consolidation law and creep constitutive model under high stress. Geotech. Test. J. 41 (2), 390–402.
Williams, T.J., Denton, D.K., Larson, M.K., Rains, R.L., Seymour, J.B., Tesarik, D.R., 2001. Geomechanics of Reinforced Cemented Backfill in an Underhand Stope at the Lucky Friday Mine. U.S. Department of Health and Human Services, Public Health Service, Centers for Disease Control and Prevention, National Institute for Occupational Safety and Health, Mullan, Idaho. Publication No. 138.
Wu, A., Ruan, Z., Wang, J., 2022. Rheological behavior of paste in metal mines. Int. J. Min., Metal. Mat. 29 (4), 717–726.
Wu, A., Yang, Y., Chen, H., Chen, S., Han, Y., 2018. Status and prospects of paste technology in China. Chin. J. Eng. 40 (5), 517–525.
Wu, D., Fall, M., Cai, S., 2014. Numerical modelling of thermally and hydraulically coupled processes in hydrating cemented tailings backfill columns. Int. J. Min. Reclamat. Environ. 28 (3), 173–199.
Wu, D., Liu, L., Yilmaz, E., Zheng, S., 2025. Numerical prediction of strength and temperature changes within cemented paste backfill considering barricade stability. Eng. Sci. Technol. 62, 101966.
Xu, W., Zhang, Y., Zuo, X., Hong, M., 2020. Time-dependent rheological and mechanical properties of silica fume modified cemented tailings backfill in low temperature environment. Cement Concr. Compos. 114, 103804.
Xue, G., Yilmaz, E., Wang, Y., 2023. Progress and prospects of mining with backfill in metal mines in China. Int. J. Min. Metal. Mat. 30 (8), 1455–1473.
Yan, B., Jia, H., Liu, Y., Liu, P., Yilmaz, E., 2025. Revealing cooperative load-bearing mechanisms between mine backfill and rock pillar using a bonded-block modeling approach. Minerals 15 (3), 210.
Yang, L., Li, J., Liu, H., Jiao, H., Yin, S., Chen, X., Yu, Y., 2023. Systematic review of mixing technology for recycling waste tailings as cemented paste backfill in mines in China. Int. J. Min. Metal. Mat. 30 (8), 1430–1443.
Yang, S., Wang, H., Ruan, Z., Liu, H., 2024. Dynamic response and deformation failure microscopic characteristics of cyclic impact–cemented tailing backfill. Environ. Sci. Pollut. Res. 31 (30), 42857–42874.
Yang, Y., Chen, Z., Feng, W., Nong, Y., Yao, M., Tang, Y., 2021. Shrinkage compensation design and mechanism of geopolymer pastes. Constr. Build. Mater. 299, 123916.
Yilmaz, E., Belem, T., Benzaazoua, M., 2014. Effects of curing and stress conditions on hydromechanical, geotechnical and geochemical properties of cemented paste backfill. Eng. Geol. 168, 23–37.
Yilmaz, E., Belem, T., Bussière, B., Benzaazoua, M., 2008. Consolidation characteristics of early age cemented paste backfill. In: Proceedings of the 61st Canadian Geotechnical Conference and the 9th Joint CGS/IAH-CNC Groundwater Conference, Edmonton, Alberta, Canada, pp. 797–804.
Yilmaz, E., Belem, T., Bussière, B., Mbonimpa, M., Benzaazoua, M., 2015. Curing time effect on consolidation behaviour of cemented paste backfill containing different cement types and contents. Constr. Build. Mater. 75, 99–111.
Yin, S., Hou, Y., Chen, X., Zhang, M., 2021. Mechanical, flowing and microstructural properties of cemented sulfur tailings backfill: effects of fiber lengths and dosage. Constr. Build. Mater. 309, 125058.
Yin, S., Shao, Y., Wu, A., Wang, H., Liu, X., Wang, Y., 2020. A systematic review of paste technology in metal mines for cleaner production in China. J. Clean. Prod. 247, 119590.
Zhao, X., Fourie, A., Qi, C., 2020. Mechanics and safety issues in tailing-based backfill: a review. Int. J. Miner. Metall. Mater. 27 (9), 1165–1178.
Zhao, Y., Taheri, A., Karakus, M., Deng, A., Guo, L., 2021. The effect of curing under applied stress on the mechanical performance of cement paste backfill. Minerals 11 (10), 1107.
Zhou, Q., Beaudoin, J.J., 2003. Effect of applied hydrostatic stress on the hydration of Portland cement and C3S. Adv. Cement Res. 15 (1), 9–16.
Zhou, Y., Fall, M., 2023. Mechanical and microstructural properties of cemented paste backfill with chloride-free antifreeze additives in subzero environments. J. Mater. Civ. Eng. 35 (6), 04023148.

Prof. Mamadou Fall is a Distinguished University Professor and Head of the Civil Engineering Department at the University of Ottawa. He holds the University Research Chair in Geotechnical Engineering for Net Zero Transitions and is a Fellow of the Canadian Institute of Engineering. Prof. Fall and his research team conduct cutting-edge studies in geotechnical and geoenvironmental engineering, collaborating closely with industry, major federal and provincial institutions, and international partners. Prof. Fall has authored over 325 publications, and his research contributions have influenced engineering practice and earned him top honors, including the John B. Stirling Medal, the uOttawa Research Excellence Award, and recognition among the top 1 % of global scientists. He has also held major leadership roles in the Canadian Geotechnical Society and continues to serve the profession through expert panels, editorial boards, and conference leadership.